

Collider phenomenology of unparticle physics

Kingman Cheung,^{1,2} Wai-Yee Keung,³ and Tzu-Chiang Yuan¹

¹*Department of Physics, National Tsing Hua University, Hsinchu 300, Taiwan*

²*Physics Division, National Center for Theoretical Sciences, Hsinchu 300, Taiwan*

³*Department of Physics, University of Illinois, Chicago, Illinois 60607-7059, USA*

(Received 2 July 2007; published 12 September 2007)

Low-energy phenomenology of the unparticle physics associated with an exact scale invariant sector possessing a nontrivial infrared fixed point at a higher energy scale is explored for both electron-positron and hadronic colliders. Feynman rules for a spin 0, 1, or 2 unparticle coupled to a variety of standard model gauge invariant operators that are relevant to many low-energy processes involving either real emissions of unparticles or their virtual propagator effects are presented. Missing energy and/or recoil mass distributions of the unparticle in the associated production of the unparticle together with a photon or Z boson at LEP2 and ILC as well as in Z decay into an unparticle plus a fermion-antifermion pair are studied. In addition, monojet production with missing energy from the unparticle at hadronic collisions are explored. The complex phase in the unparticle propagator that can give rise to interesting interference effects between an unparticle-exchange diagram and the standard model amplitudes are studied in details for the Drell-Yan process as well as muon pair and diphoton production in electron-positron annihilation. These energy and/or recoil mass distributions (with the exception in hadron colliders) and interference effects are found sensitively depending not only on the scaling dimension but also on the spin of the unparticle. For the spin-2 unparticle, its physical effects are found to resemble that of a tower of Kaluza-Klein gravitons, which strongly indicates that the underlying unparticle physics may have root in a higher dimensional theory. A connection between unparticle physics and theories of large extra dimensions is speculated. Experimental constraints on the unparticle scale are deduced from the LEP2 data on monophoton production and from the 4-fermion contact interactions.

DOI: [10.1103/PhysRevD.76.055003](https://doi.org/10.1103/PhysRevD.76.055003)

PACS numbers: 14.80.-j, 12.38.Qk, 12.90.+b, 13.40.Em

I. INTRODUCTION

Scale invariance is a very appealing symmetry in both physics and mathematics. The dilatation generator D for scale transformation does not commute with the spacetime translation generators P_μ . Their commutation relations are familiar:

$$[D, P_\mu] = -iP_\mu. \quad (1)$$

This implies for a real s

$$\exp(+isD)P^2\exp(-isD) = \exp(2s)P^2. \quad (2)$$

Thus, the exact scale symmetry requires that the mass spectrum is either continuous or all masses are zero. In a renormalizable theory, this symmetry must be broken either explicitly by some dimensional mass parameters in the theory or implicitly by quantum loop effects, *à la* Coleman-Weinberg mechanism [1], for example. Indeed, scale invariance is manifestly broken in the Lagrangian of the standard model (SM) of particle physics at tree level by just a single negative mass-squared term in the Higgs potential. Despite the lack of scale invariance in the standard model, it is logically plausible to imagine that there exists such a scale invariant sector at a higher scale above TeV that can be probed at the LHC or ILC. Such a sector might be strongly coupled to itself and highly nontrivial but nevertheless can be only weakly coupled to the matter in the standard model. One expects that such a sector decouples effectively from the low energy and can use

the power of the effective field theory approach to describe its low-energy effects.

Recently, Georgi [2] motivated by the Banks-Zaks theory [3], suggested that a scale invariant sector with a nontrivial infrared fixed-point behaves rather peculiar from the perspective of particle physics. It was keenly observed in [2] that an operator \mathcal{O}_U with a general nonintegral scaling dimension d_U in a scale invariant sector has a mass spectrum that looked like a d_U number of invisible massless particles. This was coined as an unparticle \mathcal{U} by Georgi. An unparticle does not have a fixed invariant mass squared but instead a continuous mass spectrum in accordance with the above general argument. It was also pointed out that real production of an unparticle at low-energy processes described by an effective field theory can give rise to peculiar missing energy distributions because of the possible nonintegral values of d_U .

Subsequently, the propagator for the unparticle was worked out independently in [4,5]. An unusual phase in the unparticle propagator was discovered by both groups and the interesting interference patterns between the amplitude of s -channel unparticle exchange and those from the SM were studied. In Ref. [4], the interference effect between the complex phase of the unparticle propagator and the complex Breit-Wigner form of the unstable Z boson propagator was studied in detail for the backward-forward asymmetry in the $e^-e^+ \rightarrow \mu^-\mu^+$ process near the Z pole. In Ref. [5], the interference between the amplitude of an s -channel spin-1 unparticle exchange with the

SM amplitudes for the Drell-Yan process was explored at the Tevatron. A one-loop unparticle-exchange contribution to the lepton anomalous magnetic moment was also calculated in [5]. More recently, various phenomenology of the unparticle has been explored by many groups [6–24].

In this paper, we present in much more detail the results reported earlier in [5] and extend to further processes that are relevant to collider experiments. We believe these processes are of immediate interests to theoretical and experimental communities. In the next section, we review the derivation of the two-point functions [2], propagators [4,5], and spin structures of the unparticle operators $O_{\mathcal{U}}$, $O_{\mathcal{U}}^{\mu}$, and $O_{\mathcal{U}}^{\mu\nu}$ first introduced in Ref. [2]. Feynman rules for these operators coupled to those standard model invariant operators of special interests are explicitly given. In addition, four-fermion contact interactions due to spin-1 and 2 unparticle exchanges are written down. At the end of this section, we also speculate on a possible connection between unparticle physics and theories of large extra dimensions. The subsequent two sections are phenomenological applications. In Sec. III, we discuss real emissions of unparticles. This covers $e^-e^+ \rightarrow \gamma\mathcal{U}$ and $e^-e^+ \rightarrow Z\mathcal{U}$ at e^-e^+ colliders, and $Z \rightarrow f\bar{f}\mathcal{U}$ at the Z pole, as well as monojet production plus the unparticle \mathcal{U} at hadron colliders. LEP2 data of monophoton production is used to constrain the unparticle scale. In Sec. IV, we study the interference effects between the exchange of a virtual unparticle and the standard model amplitudes. We discuss several classic reactions including Drell-Yan process, $e^-e^+ \rightarrow f\bar{f}$ with $f \neq e$, and $f\bar{f} \rightarrow \gamma\gamma$. Experimental limits of the 4-fermion contact interactions from global fits are also used to constrain the unparticle scale. Conclusions and comments will be given in Sec. V. Some tedious formulas are relegated in an appendix.

II. FORMALISM

To fix notation we denote the scale invariant sector as a Banks-Zaks (\mathcal{BZ}) sector [3] and follow closely the scenario studied in [2]. The \mathcal{BZ} sector can interact with the standard model fields through the exchange of a connector sector that has a high mass scale $M_{\mathcal{U}}$. Below this high mass scale, nonrenormalizable operators that are suppressed by inverse powers of $M_{\mathcal{U}}$ are induced. Generically, we have operators of the form

$$\frac{1}{M_{\mathcal{U}}^{d_{SM}+d_{\mathcal{BZ}}-4}} \mathcal{O}_{SM} \mathcal{O}_{\mathcal{BZ}}, \quad (3)$$

where \mathcal{O}_{SM} and $\mathcal{O}_{\mathcal{BZ}}$ represent local operators constructed out of the standard model and \mathcal{BZ} fields with scaling dimensions d_{SM} and $d_{\mathcal{BZ}}$, respectively. As in massless non-Abelian gauge theories, renormalization effects in the scale invariant \mathcal{BZ} sector induce dimensional transmutation [1] at an energy scale $\Lambda_{\mathcal{U}}$. Below $\Lambda_{\mathcal{U}}$ matching conditions must be imposed onto the operator (3) to match a new set of operators having the following form

$$C_{\mathcal{O}_{\mathcal{U}}} \frac{\Lambda_{\mathcal{BZ}}^{d_{\mathcal{BZ}}-d_{\mathcal{U}}}}{M_{\mathcal{U}}^{d_{SM}+d_{\mathcal{BZ}}-4}} \mathcal{O}_{SM} \mathcal{O}_{\mathcal{U}}, \quad (4)$$

where $d_{\mathcal{U}}$ is the scaling dimension of the unparticle operator $\mathcal{O}_{\mathcal{U}}$ and $C_{\mathcal{O}_{\mathcal{U}}}$ is a coefficient function fixed by the matching. Whether this matching can be implemented is highly nontrivial since the scale invariant sector might be strongly coupled. While we are very much ignorant of this scale invariant sector above the TeV scale, it was argued in [2] that using the effective field theory approach specified by the operators like Eq. (4) one should be able to probe the unparticle physics at the LHC and ILC. Throughout this work, it is tacitly assumed that an exact scale invariance sector survives all the way down to the electroweak scale.

Three unparticle operators with different Lorentz structures were addressed in [2]: $\{O_{\mathcal{U}}, O_{\mathcal{U}}^{\mu}, O_{\mathcal{U}}^{\mu\nu}\} \in \mathcal{O}_{\mathcal{U}}$, which correspond to scalar, vector, and tensor operators, respectively. The spin- $\frac{1}{2}$ unparticle operator was considered in [6]. In general, an unparticle operator from a scale invariant sector can be labeled by a triple $(d_{\mathcal{U}}; j_1, j_2)$ where $d_{\mathcal{U}}$ is its scaling dimension and $2j_1$ and $2j_2$ are two integers labeling the representation of the Lorentz group that it belongs to. Unitarity imposes constraints on possible values taken by the scaling dimension depending on j_1 and j_2 [25]. For example, for the scalar unparticle operator $O_{\mathcal{U}}$, $j_1 = j_2 = 0$ and unitarity constrains $d_{\mathcal{U}} > 1$. In the numerical works presented in this paper, we will simply require $d_{\mathcal{U}} > 1$ for all unparticle operators. These unparticle operators can even carry standard model quantum numbers [2], for example, a charged unparticle can be anticipated. Throughout this work we are contented with the unparticle operators that are standard model singlets.

A. Phase space for real emission of an unparticle

It was demonstrated in [2] that scale invariance can be used to fix the two-point functions of the unparticle operators. Let us consider a two-point function for a scalar unparticle operator $O_{\mathcal{U}}$

$$\begin{aligned} \langle 0|O_{\mathcal{U}}(x)O_{\mathcal{U}}^{\dagger}(0)|0\rangle &= \langle 0|e^{i\hat{P}\cdot x}O_{\mathcal{U}}(0)e^{-i\hat{P}\cdot x}O_{\mathcal{U}}^{\dagger}(0)|0\rangle \\ &= \int d\lambda \int d\lambda' \langle 0|O_{\mathcal{U}}(0)|\lambda'\rangle \\ &\quad \times \langle \lambda'|e^{-i\hat{P}\cdot x}|\lambda\rangle \langle \lambda|O_{\mathcal{U}}^{\dagger}(0)|0\rangle \\ &= \int \frac{d^4P}{(2\pi)^4} e^{-iP\cdot x} \rho_{\mathcal{U}}(P^2), \end{aligned} \quad (5)$$

where $\rho_{\mathcal{U}}(P^2)$ is the spectral density and is formally given by

$$\rho_{\mathcal{U}}(P^2) = (2\pi)^4 \int d\lambda \delta^4(P - p_{\lambda}) |\langle 0|O_{\mathcal{U}}(0)|\lambda\rangle|^2. \quad (6)$$

Inverse Fourier transformation gives

$$\begin{aligned}\rho_U(P^2) &= \int d^4x e^{iP \cdot x} \langle 0 | O_U(x) O_U^\dagger(0) | 0 \rangle \\ &= A_{d_U} \theta(P^0) \theta(P^2) (P^2)^\alpha,\end{aligned}\quad (7)$$

where α is an index to be determined based on scale invariance and A_{d_U} is a normalization factor also required to be fixed. Under a scale transformation $x \rightarrow sx$ and $O_U(sx) \rightarrow s^{-d_U} O_U(x)$, we have

$$\begin{aligned}A_{d_U} \theta(P^0) \theta(P^2) (P^2)^\alpha &= \int d^4x s^4 e^{isP \cdot x} \langle 0 | s^{-2d_U} O_U(x) \\ &\quad \times O_U^\dagger(0) | 0 \rangle \\ &= s^{-2(d_U-2)} A_{d_U} \theta(sP^0) \theta(s^2P^2) \\ &\quad \times (s^2P^2)^\alpha.\end{aligned}\quad (8)$$

Requiring scale invariance implies $\alpha = d_U - 2$, since the step functions are invariant. Therefore, we obtain

$$\rho_U(P^2) = A_{d_U} \theta(P^0) \theta(P^2) (P^2)^{d_U-2} \geq 0, \quad (9)$$

where A_{d_U} is normalized to interpolate the d_U -body phase space of the massless particle [2]. The phase-space factor for the n massless particle with $(p_1 + p_2 + \dots + p_n)^2 = s^2$ and $p_i^2 = 0$ can be written as

$$dLIPS_n = A_n s^{n-2}, \quad A_n = \frac{16\pi^2 \sqrt{\pi}}{(2\pi)^{2n}} \frac{\Gamma(n + \frac{1}{2})}{\Gamma(n-1)\Gamma(2n)}, \quad (10)$$

which for the first few n 's are $A_{n-1} \rightarrow 2\pi(n-1)$, $A_2 = \frac{1}{8\pi}$ and $A_3 = \frac{1}{256\pi^3}$, etc. Based on the similar scale dependence, the unparticle spectral density is identified with the phase space of the d_U -body massless particle in a convention advocated in [2]: $d_U \rightarrow n$ and $A_n \rightarrow A_{d_U}$. So the factor A_{d_U} in Eq. (8) is given by

$$A_{d_U} = \frac{16\pi^2 \sqrt{\pi}}{(2\pi)^{2d_U}} \frac{\Gamma(d_U + \frac{1}{2})}{\Gamma(d_U-1)\Gamma(2d_U)}. \quad (11)$$

Note that d_U can now take on a nonintegral value as well. This is a peculiar feature of unparticle physics since one can now speak of something like fractional particles.

The differential cross section for a process involving the collision of two massless particles in the initial state and producing an unparticle plus a few other massless particles in the final state can be written as

$$d\sigma(p_1, p_2 \rightarrow P_U, k_1, k_2, \dots) = \frac{1}{2s} |\overline{\mathcal{M}}|^2 d\Phi,$$

where

$$\begin{aligned}d\Phi &= (2\pi)^4 \delta^{(4)}(p_1 + p_2 - P_U - k_1 - k_2 - \dots) \\ &\quad \times \prod_i \left[2\pi \theta(k_i^0) \delta(k_i^2) \frac{d^4k_i}{(2\pi)^4} \right] \\ &\quad \times A_{d_U} \theta(P_U^0) \theta(P_U^2) (P_U^2)^{d_U-2} \frac{d^4P_U}{(2\pi)^4}\end{aligned}\quad (12)$$

with $s = (p_1 + p_2)^2$ and $|\overline{\mathcal{M}}|^2$ is a spin- and color-averaged matrix element squared. Note that in the limit $d_U \rightarrow 1$ from above

$$\lim_{d_U \rightarrow 1^+} A_{d_U} (P_U^2)^{d_U-2} \theta(P_U^0) \theta(P_U^2) = 2\pi \theta(P_U^0) \delta(P_U^2), \quad (13)$$

so that the phase-space factor associated with the unparticle behaves just like a single massless particle in this limit. If there are only one massless particle and an unparticle in the final state, the phase-space factor is further simplified to

$$d\Phi = \frac{1}{2(2\pi)^3} A_{d_U} \theta(P_U^0) \theta(P_U^2) (P_U^2)^{d_U-2} k_1^0 dk_1^0 d\Omega. \quad (14)$$

B. Virtual propagator of the unparticle

The derivation of the virtual unparticle propagator is also based on scale invariance. Without loss of generality we consider a scalar propagator. The extensions to spin-1 and spin-2 propagators simply include the appropriate spin structures and will be presented in the next subsection. The Feynman propagator $\Delta_F(P^2)$ of the unparticle is determined by the spectral formula

$$\Delta_F(P^2) = \frac{1}{2\pi} \int_0^\infty \frac{R(M^2) dM^2}{P^2 - M^2 + i\epsilon} \quad (15)$$

$$= \frac{1}{2\pi} \int_0^\infty \frac{R(M^2) dM^2}{P^2 - M^2} - i \frac{1}{2} R(P^2) \theta(P^2), \quad (16)$$

where $R(M^2) = A_{d_U} (M^2)^{d_U-2}$ is the spectral density given in Eq. (9). The appropriate form for $\Delta_F(P^2)$ to be scale invariant is $\Delta_F(P^2) = Z_{d_U} (-P^2)^{d_U-2}$, where Z_{d_U} is the factor to be determined. Note that our polar angle of complex number is restricted to $[-\pi, \pi)$. The complex function $(-P^2)^{d_U-2}$ is analytic for negative P^2 , but needs a branch cut for positive P^2 :

$$(-P^2)^{d_U-2} = \begin{cases} |P^2|^{d_U-2} & \text{if } P^2 \text{ is negative and real,} \\ |P^2|^{d_U-2} e^{-id_U\pi} & \text{for positive } P^2 \text{ with an infinitesimal } i0^+. \end{cases} \quad (17)$$

This choice guarantees a propagator with a spacelike momentum is real without cuts. We can then determine the factor Z_{d_u} by comparing with the imaginary part of $\Delta_F(P^2)$ for a timelike momentum ($P^2 > 0$):

$$\begin{aligned}\Im\Delta_F(P^2) &= -Z_{d_u} \sin(d_u\pi)(P^2)^{d_u-2} \\ &= -\frac{1}{2}A_{d_u}(P^2)^{d_u-2}.\end{aligned}\quad (18)$$

We thus obtain

$$Z_{d_u} = \frac{A_{d_u}}{2 \sin(d_u\pi)}, \quad (19)$$

and the unparticle propagator is given by

$$\Delta_F(P^2) = \frac{A_{d_u}}{2 \sin(d_u\pi)} (-P^2)^{d_u-2}, \quad (20)$$

where the definition of $(-P^2)^{d_u-2}$ is given in Eq. (17). In a t - or u -channel process, $(-P^2)$ is positive and so there is no complex phase associated with the propagator. On the other hand, for an s -channel process $(-P^2)$ is negative and so there is a complex phase associated with the propagator. This will lead to interesting interference effects with the standard model amplitudes. For instance, in $e^-e^+ \rightarrow \mu^-\mu^+$ [4] or Drell-Yan process [5], the unparticle propagator can interfere with the real photon propagator and with both the real and imaginary parts of the unstable Z boson propagator. We note that since $Z_{d_u} \rightarrow -1$ as $d_u \rightarrow 1^+$, Eq. (20) reproduces the familiar result

$$\lim_{d_u \rightarrow 1^+} \Delta_F(P^2) = \frac{1}{P^2}. \quad (21)$$

C. Spin structures of unparticle operators

In Eq. (9), the operator O_u is a scalar. It is straightforward to extend to spin-1 and spin-2 unparticle operators by including appropriate tensor structures:

$$\begin{aligned}\langle 0|O_u^\mu(x)O_u^{\nu\dagger}(0)|0\rangle &= A_{d_u} \int \frac{d^4P}{(2\pi)^4} e^{-iP\cdot x} \theta(P^0) \theta(P^2) \\ &\quad \times (P^2)^{d_u-2} \pi^{\mu\nu}(P),\end{aligned}\quad (22)$$

$$\begin{aligned}\langle 0|O_u^{\mu\nu}(x)O_u^{\rho\sigma\dagger}(0)|0\rangle &= A_{d_u} \int \frac{d^4P}{(2\pi)^4} e^{-iP\cdot x} \theta(P^0) \theta(P^2) \\ &\quad \times (P^2)^{d_u-2} T^{\mu\nu,\rho\sigma}(P),\end{aligned}\quad (23)$$

where

$$\pi^{\mu\nu}(P) = -g^{\mu\nu} + \frac{P^\mu P^\nu}{P^2}, \quad (24)$$

$$\begin{aligned}T^{\mu\nu,\rho\sigma}(P) &= \frac{1}{2} \{ \pi^{\mu\rho}(P) \pi^{\nu\sigma}(P) + \pi^{\mu\sigma}(P) \pi^{\nu\rho}(P) \\ &\quad - \frac{2}{3} \pi^{\mu\nu}(P) \pi^{\rho\sigma}(P) \}.\end{aligned}\quad (25)$$

The forms of $\pi^{\mu\nu}(P)$ and $T^{\mu\nu,\rho\sigma}$ are chosen such that $P_\mu \pi^{\mu\nu}(P) = 0$, $P_\mu T^{\mu\nu,\rho\sigma}(P) = 0$, and $T_\mu^{\mu,\rho\sigma} = 0$. The

unparticle operators are all taken to be Hermitian, and O_u^μ and $O_u^{\mu\nu}$ are assumed to be transverse. In addition, the spin-2 unparticle operator is taken to be traceless $O_u^\mu{}_\mu = 0$. The propagators for vector and tensor operators can be derived as in Eq. (20) for the scalar case using spectral decomposition:

$$[\Delta_F(P^2)]_{\mu\nu} = \frac{A_{d_u}}{2 \sin(d_u\pi)} (-P^2)^{d_u-2} \pi_{\mu\nu}(P), \quad (26)$$

$$[\Delta_F(P^2)]_{\mu\nu,\rho\sigma} = \frac{A_{d_u}}{2 \sin(d_u\pi)} (-P^2)^{d_u-2} T_{\mu\nu,\rho\sigma}(P). \quad (27)$$

D. Effective operators

The common effective interactions that satisfy the standard model gauge symmetry for the scalar, vector, and tensor unparticle operators with standard model fields are given, respectively, by

$$\begin{aligned}\lambda_0 \frac{1}{\Lambda_u^{d_u-1}} \bar{f} f O_u, & \quad \lambda_0 \frac{1}{\Lambda_u^{d_u-1}} \bar{f} i \gamma^5 f O_u, \\ \lambda_0 \frac{1}{\Lambda_u^{d_u}} \bar{f} \gamma^\mu f (\partial_\mu O_u), & \quad \lambda_0 \frac{1}{\Lambda_u^{d_u}} G_{\alpha\beta} G^{\alpha\beta} O_u,\end{aligned}\quad (28)$$

$$\lambda_1 \frac{1}{\Lambda_u^{d_u-1}} \bar{f} \gamma_\mu f O_u^\mu, \quad \lambda_1 \frac{1}{\Lambda_u^{d_u-1}} \bar{f} \gamma_\mu \gamma_5 f O_u^\mu, \quad (29)$$

$$\begin{aligned}-\frac{1}{4} \lambda_2 \frac{1}{\Lambda_u^{d_u}} \bar{\psi} i (\gamma_\mu \vec{D}_\nu + \gamma_\nu \vec{D}_\mu) \psi O_u^{\mu\nu}, \\ \lambda_2 \frac{1}{\Lambda_u^{d_u}} G_{\mu\alpha} G_\nu^\alpha O_u^{\mu\nu},\end{aligned}\quad (30)$$

where the covariant derivative $D_\mu = \partial_\mu + ig \frac{\tau^a}{2} W_\mu^a + ig' \frac{Y}{2} B_\mu$, $G^{\alpha\beta}$ denotes the gauge field strength (gluon, photon, and weak gauge bosons), f stands for a standard model fermion, ψ stands for a standard model fermion doublet or singlet, and λ_i are dimensionless effective couplings $C_{O_u^i} \Lambda_u^{d_{BZ}} / M_{\text{SM}}^{d_{\text{SM}} + d_{BZ} - 4}$ with the index $i = 0, 1$, and 2 labeling the scalar, vector, and tensor unparticle operators, respectively. Here we label each coupling constant $\lambda_i (i = 0, 1, 2)$ the same for various operators of each spin. In principle, they can be different and they are then distinguished by additional indices. For simplicity we will also assume universality that λ_i 's are flavor blind. The Feynman rules for the operators in Eqs. (28)–(30) are shown in Figs. 1–3, respectively. Conventional wisdom tells us that the scalar operator O_u coupled to the fermion is suppressed by the fermion mass. As already studied in [2,4,5], some of the operators listed above can give rise to interesting phenomenology, including real emission of the unparticle as well as effective 4-fermion contact interactions. Phenomenology of unparticles that couple to flavor

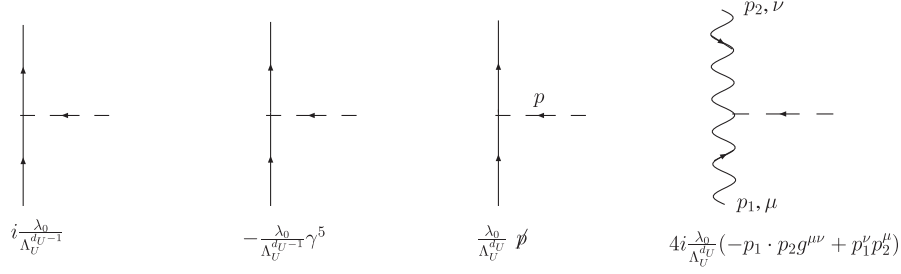


FIG. 1. Feynman rules for the scalar unparticle operators in Eq. (28).

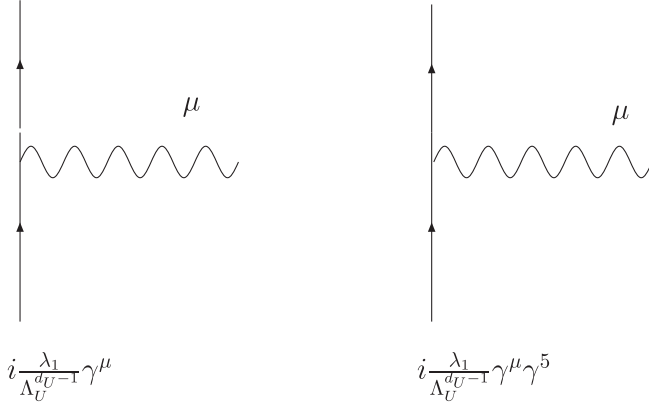


FIG. 2. Feynman rules for the vector unparticle operators in Eq. (29).

changing neutral currents have also been studied in [2,6,7,10–12,16]. More gauge invariant operators that couple the spin-0 and spin-1 unparticle operators to SM fields are listed in [17].

E. Effective four-fermion interactions

Virtual exchange of the unparticle corresponding to the vector operator $O_{\mathcal{U}}^{\mu}$ between two fermionic currents can result in the following 4-fermion interaction [Fig. 4(a)] [5]

$$\mathcal{M}_1^{4f} = \lambda_1^2 Z_{d_{\mathcal{U}}} \frac{1}{\Lambda_{\mathcal{U}}^2} \left(-\frac{P_{\mathcal{U}}^2}{\Lambda_{\mathcal{U}}^2} \right)^{d_{\mathcal{U}}-2} (\bar{f}_2 \gamma_{\mu} f_1) (\bar{f}_4 \gamma^{\mu} f_3). \quad (31)$$

The 4-momentum flowing along the unparticle propagator is $P_{\mathcal{U}} \equiv (p_1 - p_2)$. The contribution from the longitudinal piece $P_{\mathcal{U}}^{\mu} P_{\mathcal{U}}^{\nu} / P_{\mathcal{U}}^2$ in Eq. (24) has been dropped for massless external fermions. The convention of the fractional exponent of a complex number is already given in Eq. (17). The $(-)$ sign in front of $P_{\mathcal{U}}^2$ of the unparticle propagator in Eq. (31) gives rise to a phase factor $\exp(-i\pi d_{\mathcal{U}})$ for timelike momentum $P_{\mathcal{U}}^2 > 0$, but not for spacelike momentum $P_{\mathcal{U}}^2 < 0$. For example, in Drell-Yan production the virtual exchange of the unparticle in the s -channel will have $P_{\mathcal{U}}^2$ taken as the \hat{s} of the subprocess and therefore will contain a phase. The most important feature is that the high-energy behavior of the amplitude scales as $(\hat{s}/\Lambda_{\mathcal{U}}^2)^{d_{\mathcal{U}}-1}$. For $d_{\mathcal{U}} = 1$ the tree amplitude behaves like that of a massless photon exchange, while for $d_{\mathcal{U}} = 2$ the amplitude reduces to the conventional 4-fermion interaction [26,27], i.e., its high-energy behavior scales like $s/\Lambda_{\mathcal{U}}^2$. If $d_{\mathcal{U}}$ is between 1 and 2, say 3/2, the amplitude has the unusual behavior of $\sqrt{\hat{s}}/\Lambda_{\mathcal{U}}$ at high energy. If $d_{\mathcal{U}} = 3$ the amplitude's high-energy behavior becomes $(\hat{s}/\Lambda_{\mathcal{U}}^2)^2$, which resembles the exchange of a Kaluza-Klein tower of gravitons [28]. In principle, we can allow

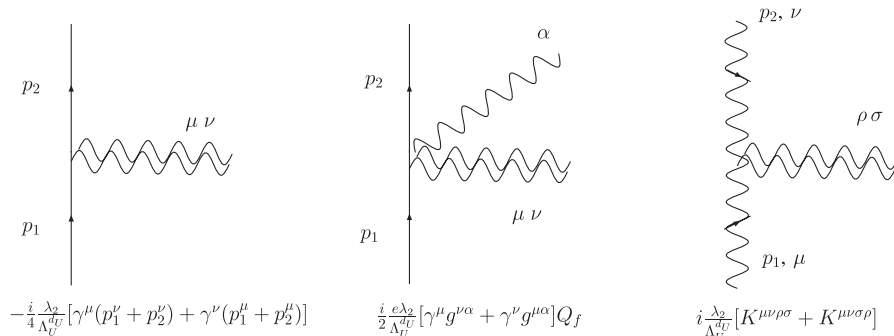


FIG. 3. Feynman rules for the tensor unparticle operators in Eq. (30). The $K^{\mu\nu\rho\sigma} = -g^{\mu\nu} p_1^{\rho} p_2^{\sigma} - p_1 \cdot p_2 g^{\rho\mu} g^{\sigma\nu} + p_1^{\nu} p_2^{\rho} g^{\sigma\mu} + p_2^{\mu} p_1^{\rho} g^{\sigma\nu}$. The double-wavy line represents a spin-2 unparticle while the single-wavy line represents a photon, and Q_f denotes the electric charge of the fermion. In case of a Z boson in the middle diagram, replace eQ_f by $\frac{g}{\cos\theta_w}(T_{3f} - Q_f \sin^2\theta_w)$, where T_{3f} is the isospin projection of the fermion doublet.

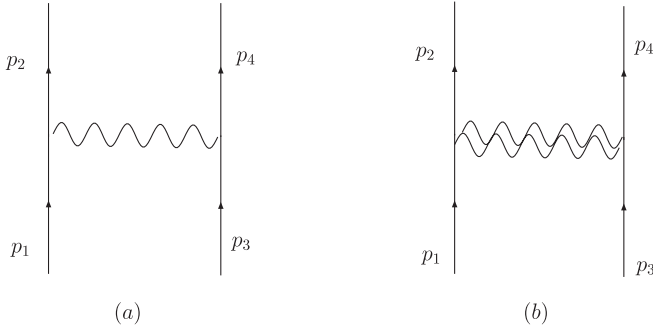


FIG. 4. Feynman diagrams for exchange of spin-1 and spin-2 unparticles between two fermionic currents.

different couplings in different chirality combinations in the 4-fermion contact interactions, denoted by LL , RR , LR , RL , which can produce parity violation and therefore the forward-backward asymmetries. The combination of $LL + RR + LR + RL$ gives VV interaction while $LL + RR - LR - RL$ gives AA interaction that corresponds to the vector and axial-vector interactions introduced in Ref. [4].

One can also consider the exchange of a spin-2 unparticle between a pair of fermionic currents. The operator is given in Eq. (30) and the Feynman rule in Fig. 3. After simplification we arrive at the following 4-fermion interaction

$$\begin{aligned} \mathcal{M}_2^{Af} = & -\frac{1}{8} \lambda_2^2 Z_{d_u} \frac{1}{\Lambda_u^4} \left(-\frac{P_u^2}{\Lambda_u^2} \right)^{d_u-2} (\bar{f}_2 \gamma^\mu f_1) (\bar{f}_4 \gamma^\nu f_3) \\ & \times [(p_1 + p_2) \cdot (p_3 + p_4) g_{\mu\nu} \\ & + (p_1 + p_2)_\nu (p_3 + p_4)_\mu], \end{aligned} \quad (32)$$

for massless external fermions, where p_i denotes the 4-momentum of the fermion f_i along the fermion line [Fig. 4(b)]. Note that the 4-fermion interaction induced by the spin-2 unparticle operator is further suppressed by $(s/\Lambda_u)^2$ relative to that induced by the spin-1 unparticle operator. This is similar to the exchange by a spin-2 graviton (which corresponds exactly when d_u is set to 2 in Eq. (32).) Similarly, different chirality combinations are possible for the 4-fermion contact interactions with spin-2 unparticle exchange.

The above 4-fermion amplitudes can interfere with the standard model amplitudes of γ , W , and Z exchange, and thus leads to interesting interference effects. In particular, the different spin structures could be differentiated by studying various angular distributions. Based on these spin-1 and spin-2 unparticle-exchange amplitudes one can study the Drell-Yan process at hadron colliders, deep-inelastic scattering at ep colliders, fermion-pair production at e^-e^+ colliders, atomic-parity violation, as well as many other low-energy eq scattering processes, just in similar ways as the conventional 4-fermion contact interactions [27] or as the Kaluza-Klein states of graviton [29].

Modification of the Newton's inverse square law in the submillimeter range due to spin-2 unparticle exchange and its possible tests at low-energy gravity experiments have been studied in [24].

F. Conjecture to large extra dimensions

The close similarity between the unparticle and Kaluza-Klein (KK) modes of the large extra dimensions [30] (LED) has been recognized [5] in the calculation of the production cross sections and in virtual effects. The unparticle and the KK states [31,32] share analogous phase-space integrations [28], in particular, the integration over the invariant mass squared P^2 . It would be interesting to relate the unparticle with the KK modes in LED.

Let us first set up all fields of the standard model to be confined on a flat 3 dimensional spatial brane with coordinates \mathbf{x} . A scalar unparticle field can be identified as a massless scalar bulk field $\Phi(t, \mathbf{x}, y)$ permeating into the LED described by extra coordinates y_i ($i = 1, \dots, n$). We study the simplest case that the space of LED is flat and periodic in each y_i with periodicity L . The massless energy-momentum relation is

$$E^2 = \mathbf{p}^2 + \sum_{i=1}^n (k_i)^2, \quad (33)$$

where \mathbf{p} is the momentum in the ordinary 3-space and k_i is the momentum component in LED. Periodic conditions on the extra dimensions require all the momenta k_i to be quantized such that they are integral multiples of $2\pi/L$. As SM physics only operates on the 3-brane, the term $\sum_{i=1}^n (k_i)^2$ of the corresponding KK modes effectively becomes the mass squared of a particle propagating in the $3 + 1$ spacetime. For large L , the summation over the KK modes turns into an integral and the density of states is introduced as

$$\sum_{\vec{k}} \rightarrow \int \left(\frac{L}{2\pi} \right)^n d^n k = \int \frac{L^n (m^2)^{(n/2-1)} dm^2}{(4\pi)^{n/2} \Gamma(\frac{n}{2})}. \quad (34)$$

Identifying the power of m^2 in the density of states with the power of P^2 in the spectral density of the unparticle, we obtain

$$d_u = \frac{n}{2} + 1. \quad (35)$$

With one extra dimension we can have the notion of one-and-a-half particle viewed from the 3-brane, and so on. It is also tempting to make the following identification

$$A_{d_u} = \frac{L^{2(d_u-1)}}{(4\pi)^{d_u-1} \Gamma(d_u-1)} \quad (36)$$

with d_u given by Eq. (35). Perhaps hidden higher dimension spacetime reveals itself through the unparticle physics. It might be interesting to see if realistic models can be built based on this alternative interpretation of the unpar-

ticle. Recently, it has been demonstrated in [33] that other values of d_U related to a dimensionless mass parameter can be achieved by deconstructing the unparticle in the 5 dimensional warped anti-de Sitter (AdS) space using the AdS/conformal field theory (CFT) correspondence.

III. PHENOMENOLOGY: REAL EMISSION

A. Monophoton and mono-Z production in e^-e^+ collisions

The energy spectrum of the monophoton from the process $e^-(p_1)e^+(p_2) \rightarrow \gamma(k_1)\mathcal{U}(P_U)$ can be used to probe the unparticle [5]. Similarly, the mono-Z production is also sensitive to the presence of some unknown particles or unparticle. Let us first derive the cross section formulas for mono-Z production.

The differential cross section for $f(p)\bar{f}(p') \rightarrow Z(k)\mathcal{U}(P_U)$ is given by

$$d\sigma = \frac{1}{2s} |\overline{\mathcal{M}}|^2 \sqrt{\frac{E_Z^2 - M_Z^2 A_{d_U}}{16\pi^3 \Lambda_U^2}} \times \left(\frac{P_U^2}{\Lambda_U^2}\right)^{d_U-2} \theta(P_U^0) \theta(P_U^2) dE_Z d\Omega_Z, \quad (37)$$

where $|\overline{\mathcal{M}}|^2$ is the spin- and color-averaged matrix element squared. Note that the invariant mass squared P_U^2 of the unparticle is not fixed but is related to the energy E_Z of the Z boson via the recoil mass relation

$$P_U^2 = s + M_Z^2 - 2\sqrt{s}E_Z, \quad (38)$$

where the energy range of E_Z is

$$M_Z \leq E_Z \leq E_Z^{\max} \equiv \frac{s + M_Z^2}{2\sqrt{s}}. \quad (39)$$

As usual, we define $s = (p + p')^2$, $t = (p - k)^2$ and $u = (p - P_U)^2$. Moreover, $s + t + u = M_Z^2 + P_U^2$.

As d_U approaches unity, we recover the on-mass-shell condition in the phase space

$$\lim_{d_U \rightarrow 1^+} A_{d_U} (P_U^2)^{d_U-2} \theta(P_U^2) = 2\pi \delta(P_U^2) = \frac{1}{2\sqrt{s}} \delta(E_Z - E_Z^{\max}). \quad (40)$$

Thus, the integral over E_Z is trivial and the cross section becomes

$$\lim_{d_U \rightarrow 1^+} d\sigma = \frac{1}{2s} \frac{1}{32\pi^2} \left(1 - \frac{M_Z^2}{s}\right) |\overline{\mathcal{M}}|_{E_Z=E_Z^{\max}}^2 d\Omega_Z. \quad (41)$$

This reproduces the usual formula for $2 \rightarrow 2$ cross section. This is expected since $d_U \rightarrow 1$ corresponds to unparticle \rightarrow particle. In this case, the energy spectrum for the Z boson is just a delta function localized at $E_Z = E_Z^{\max}$.

1. Spin-1 unparticle

Let us turn our focus back to the unparticle. For the spin-1 unparticle, we consider only the first (vectorial) operator in Eq. (29). Including the second (axial-vectorial) operator in Eq. (29) is straightforward. There are two contributing Feynman diagrams, t - and u -channels. The matrix element squared for $f(p)\bar{f}(p') \rightarrow Z(k)\mathcal{U}(P_U)$ is given by

$$|\overline{\mathcal{M}}|^2 = \frac{2}{N_c} \lambda_1^2 \frac{e^2(g_L^{f^2} + g_R^{f^2})}{\sin^2\theta_w \cos^2\theta_w} g(t/M_Z^2, u/M_Z^2, P_U^2/M_Z^2), \quad (42)$$

where N_c is the number of color for the fermion f , $g_L^f = T_{3f} - Q_f \sin^2\theta_w$, $g_R^f = -Q_f \sin^2\theta_w$ with Q_f is the electric charge of the fermion f , and the function $g(x, y, z)$ is defined by

$$g(x, y, z) = \frac{1}{2} \left(\frac{x}{y} + \frac{y}{x}\right) + \frac{(1+z)^2}{xy} - \frac{z}{2} \left(\frac{1}{x^2} + \frac{1}{y^2}\right) - (1+z) \left(\frac{1}{x} + \frac{1}{y}\right). \quad (43)$$

The result for $f(p)\bar{f}(p') \rightarrow \gamma(k)\mathcal{U}(P_U)$ can be obtained by setting M_Z equal to zero and the appropriate substitution for the couplings in Eq. (37), viz.

$$d\sigma = \frac{1}{2s} |\overline{\mathcal{M}}|^2 \frac{A_{d_U}}{16\pi^3 \Lambda_U^2} \left(\frac{P_U^2}{\Lambda_U^2}\right)^{d_U-2} E_\gamma dE_\gamma d\Omega \quad (44)$$

with the matrix element squared given by

$$|\overline{\mathcal{M}}|^2 = \frac{2}{N_c} \lambda_1^2 e^2 Q_f^2 \frac{u^2 + t^2 + 2sP_U^2}{ut}. \quad (45)$$

The P_U^2 is related to the energy of the photon E_γ by a simpler recoil mass relation,

$$P_U^2 = s - 2\sqrt{s}E_\gamma. \quad (46)$$

The monophoton energy and recoil mass distributions are plotted in Fig. 5 for various choices of d_U at $\sqrt{s} = 1$ TeV. The sensitivity of the scaling dimension to these distributions can be easily discerned. The standard model background from $e^-e^+ \rightarrow \gamma Z^* \rightarrow \gamma\nu\bar{\nu}$ is also displayed for comparison. Similar features are also found for the process $e^-e^+ \rightarrow Z\mathcal{U}$ which has also been studied recently in [17].

2. Spin-2 unparticle

We consider both spin-2 unparticle operators in Eq. (30) and let their coupling constants be different, denoted by λ_2' and λ_2 , respectively. There are four contributing Feynman diagrams for the process: t - and u -channels plus a seagull diagrams from the first operator and an s -channel diagram from the second. The matrix element squared for $f(p)\bar{f}(p') \rightarrow Z(k)\mathcal{U}(P_U)$ is given by

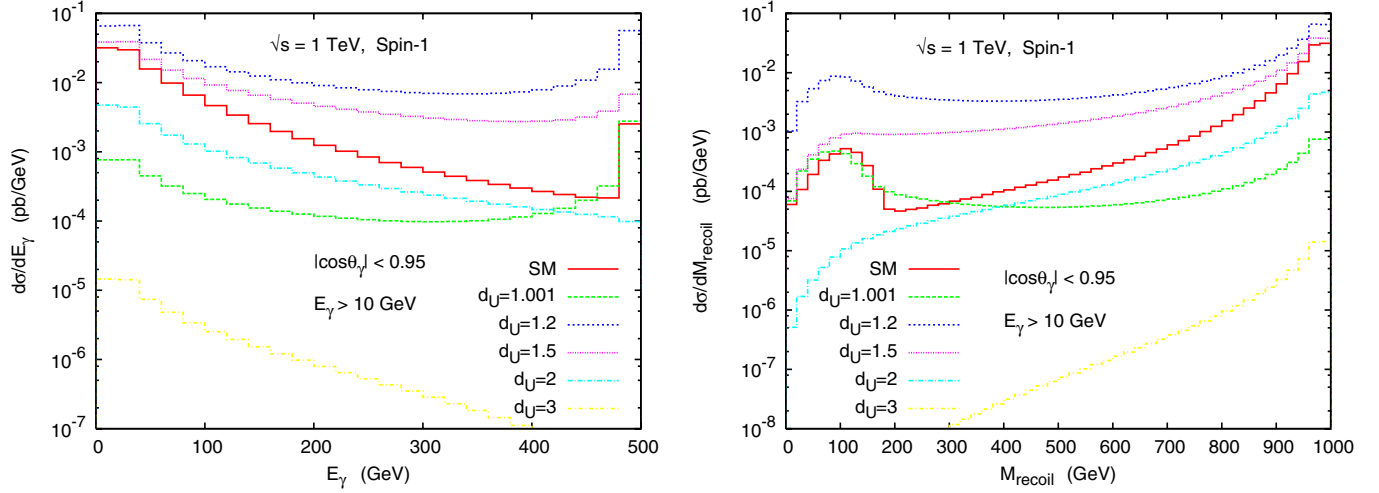


FIG. 5 (color online). Comparison of photon energy and recoil mass distributions of $e^-e^+ \rightarrow \gamma\mathcal{U}$ (spin-1 unparticle) with the standard model background $e^-e^+ \rightarrow \gamma Z^* \rightarrow \gamma\nu\bar{\nu}$ for different values of $d_{\mathcal{U}} = 1.001, 1.2, 1.5, 2,$ and 3 at $\sqrt{s} = 1$ TeV.

$$|\overline{\mathcal{M}}|^2 = \frac{1}{4N_c} \frac{\lambda_2^2}{\Lambda_{\mathcal{U}}^2} \frac{e^2(g_L^2 + g_R^2)}{2\sin^2\theta_w \cos^2\theta_w} \frac{1}{3(s - M_Z^2)^2 t^2 u^2} \times [F(t, u) + rG(t, u) + r^2H(t, u)] \quad (47)$$

with $r = \lambda'_2/\lambda_2$ and

$$(F, G, H) = (F_0, G_0, H_0) + \frac{1}{P_{\mathcal{U}}^2} (F_2, G_2, H_2) + \frac{1}{P_{\mathcal{U}}^4} (F_4, G_4, H_4), \quad (48)$$

where these complicated functions can be found in the appendix. We note that these functions satisfy the following equations

$$F_2 + G_2 + H_2 = 0, \quad F_4 + G_4 + H_4 = 0.$$

Thus, if we set $r = 1$, i.e., $\lambda_2 = \lambda'_2$, the $1/P_{\mathcal{U}}^2$ and $1/P_{\mathcal{U}}^4$ terms in the matrix element squared summed up to zero. This simply reflects the fact that longitudinal parts in the polarization sum of the spin-2 unparticle, just like the Z boson case, make no contribution to the matrix elements since the external fermion masses have been set to be zero in our calculation. In the case of $r = 1$, the above matrix element squared is simplified to

$$|\overline{\mathcal{M}}|^2 = \frac{1}{4N_c} \frac{\lambda_2^2}{\Lambda_{\mathcal{U}}^2} \frac{e^2(g_L^2 + g_R^2)}{2\sin^2\theta_w \cos^2\theta_w} \frac{1}{3(s - M_Z^2)^2 t^2 u^2} \mathcal{F}(t, u), \quad (49)$$

where

$$\begin{aligned} \mathcal{F} &\equiv F_0 + G_0 + H_0 \\ &= 8M_Z^6 tu [3P_{\mathcal{U}}^4 + 4tu - 3P_{\mathcal{U}}^2(t+u)] + 3tu(-P_{\mathcal{U}}^2 + t+u)[2P_{\mathcal{U}}^4 + t^2 + u^2 - 2P_{\mathcal{U}}^2(t+u)] \\ &\quad \times [-P_{\mathcal{U}}^4 - 4tu + P_{\mathcal{U}}^2(t+u)] + 2M_Z^4 tu [27P_{\mathcal{U}}^6 - 42P_{\mathcal{U}}^4(t+u) - 28tu(t+u) + 5P_{\mathcal{U}}^2(3t^2 + 16tu + 3u^2)] \\ &\quad + M_Z^2 [52t^3 u^3 + 36t^2 u^2(t^2 + u^2) - 3P_{\mathcal{U}}^8(t^2 - 12tu + u^2) - 6P_{\mathcal{U}}^6 tu(t^3 + 23t^2 u + 23tu^2 + u^3) \\ &\quad - 3P_{\mathcal{U}}^4(t^4 - 14t^3 u - 62t^2 u^2 - 14tu^3 + u^4) + 6P_{\mathcal{U}}^6(t^3 + u^3 - 12tu(t+u))]. \end{aligned} \quad (50)$$

Equations (49) and (50) coincide with the matrix element for $f\bar{f} \rightarrow ZG$ where G is the Kaluza-Klein graviton obtained previously in [34]. Setting $r = 1$ implies that the two operators in Eq. (30) sum up and have the form of the energy-momentum stress tensor in flat spacetime. This idea has been generalized to curved spacetime [24].

Just like the spin-1 case, we can obtain $f(p)\bar{f}(p') \rightarrow \gamma(k)\mathcal{U}(P_{\mathcal{U}})$ with appropriate substitutions:

$$|\overline{\mathcal{M}}|^2 = \frac{1}{4N_c} \frac{\lambda_2^2}{\Lambda_{\mathcal{U}}^2} e^2 Q_f^2 \frac{1}{3s^2 t^2 u^2} \times [F(t, u) + rG(t, u) + r^2H(t, u)], \quad (51)$$

where $F, G,$ and H are given by the previous formulas with M_Z setting to zero. In the case of $r = 1$, the matrix element squared reduces to

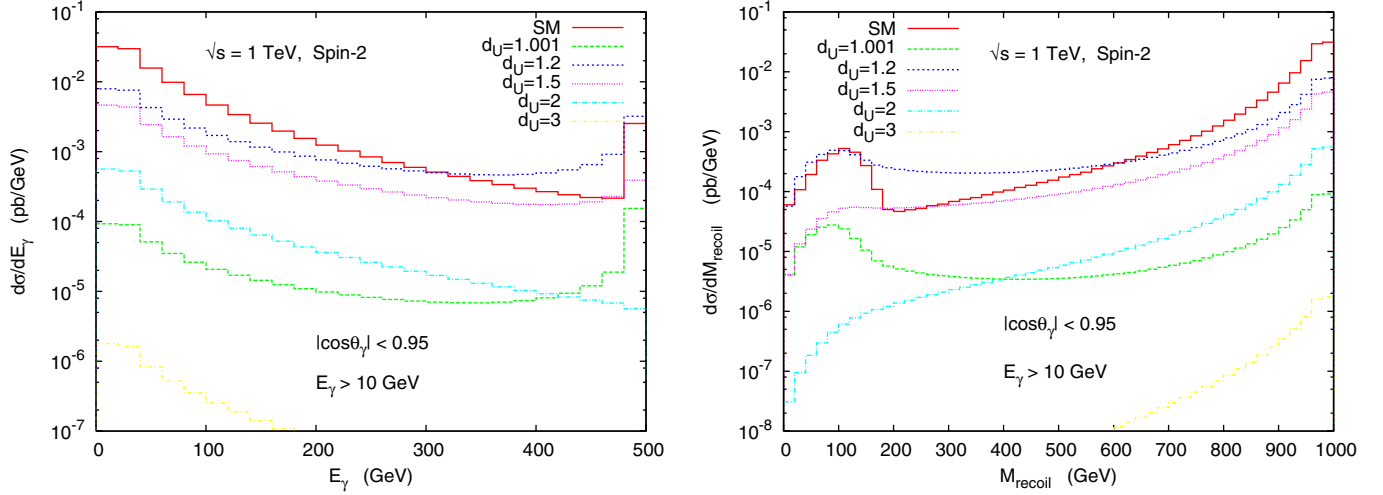


FIG. 6 (color online). Comparison of photon energy and recoil mass distributions of $e^-e^+ \rightarrow \gamma\mathcal{U}$ (spin-2 unparticle) with the standard model background $e^-e^+ \rightarrow \gamma Z^* \rightarrow \gamma\nu\bar{\nu}$ for different values of $d_{\mathcal{U}} = 1.001, 1.2, 1.5, 2,$ and 3 at $\sqrt{s} = 1$ TeV.

$$|\overline{\mathcal{M}}|^2 = \frac{1}{4N_c} \frac{\lambda_2^2}{\Lambda_{\mathcal{U}}^2} e^2 Q_f^2 \frac{1}{stu} (2sP_{\mathcal{U}}^2 + t^2 + u^2)(sP_{\mathcal{U}}^2 + 4tu). \quad (52)$$

The monophoton energy and recoil mass distributions for emission of the spin-2 unparticle are plotted in Fig. 6 for various choices of $d_{\mathcal{U}}$ at $\sqrt{s} = 1$ TeV with $r = 1$. The sensitivity of the scaling dimension to these distributions can be also easily discerned. The standard model background from $e^-e^+ \rightarrow \gamma Z^* \rightarrow \gamma\nu\bar{\nu}$ is also displayed for comparison. Similar features are also found for the process $e^-e^+ \rightarrow Z\mathcal{U}$ for the spin-2 case.

B. $Z \rightarrow f\bar{f}\mathcal{U}$

The decay width for the process $Z \rightarrow f\bar{f}\mathcal{U}$ with a spin-1 unparticle can be easily obtained as [5]

$$\frac{d\Gamma(Z \rightarrow f\bar{f} + \mathcal{U})}{dx_1 dx_2 d\xi} = \Gamma(Z \rightarrow f\bar{f}) \frac{\lambda_1^2}{8\pi^3} g(1-x_1, 1-x_2, \xi) \times \frac{M_Z^2}{\Lambda_{\mathcal{U}}^2} A_{d_{\mathcal{U}}} \left(\frac{P_{\mathcal{U}}^2}{\Lambda_{\mathcal{U}}^2} \right)^{d_{\mathcal{U}}-2}, \quad (53)$$

where $\xi = P_{\mathcal{U}}^2/M_Z^2$ and $x_{1,2}$ are the energy fractions of the fermions $x_{1,2} = 2E_{f,\bar{f}}/M_Z$. The function $g(z, w, \xi)$ has been defined in Eq. (43). The integration domain for Eq. (53) is defined by $0 < \xi < 1$, $0 < x_1 < 1 - \xi$, and $1 - x_1 - \xi < x_2 < (1 - x_1 - \xi)/(1 - x_1)$. In [5], we plotted the normalized decay rate of this process versus the energy fraction of the fermion x_1 . Here, in Fig. 7, we plot the normalized decay rate of this process versus the energy fraction of the unparticle $x_3 = 2 - x_1 - x_2$. One can see that the shape depends sensitively on the scaling dimension of the unparticle operator. As $d_{\mathcal{U}} \rightarrow 1$, the result approaches a familiar case of $\gamma^* \rightarrow q\bar{q}g^*$ [35]. The matrix element squared for $Z \rightarrow f\bar{f}\mathcal{U}$ with a spin-2 unparticle can

be obtained by applying crossing symmetry to the formulas for $f\bar{f} \rightarrow Z\mathcal{U}$ given in Eqs. (49) and (50). We omit the detailed formulas here.

C. Monojet production at hadronic collisions

It was suggested in [2] that in hadronic collisions the following partonic subprocesses which can lead to monojet signals could be important for detection of the unparticle.

$$gg \rightarrow g\mathcal{U}, \quad q\bar{q} \rightarrow g\mathcal{U}, \quad qg \rightarrow q\mathcal{U}, \quad \bar{q}g \rightarrow \bar{q}\mathcal{U}.$$

For the subprocesses that involve both quark and gluon, we consider solely the effects from the vector operator $O_{\mathcal{U}}^\mu$. For the gluon-gluon fusion subprocess, we consider solely the effects from the scalar operator $O_{\mathcal{U}}$. The partonic cross section can be derived as

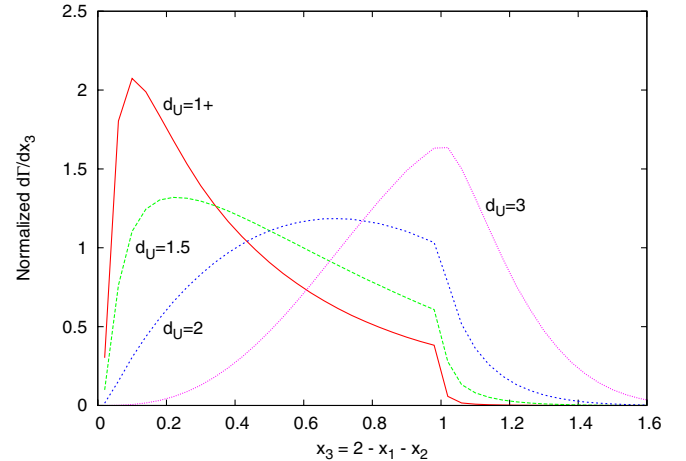


FIG. 7 (color online). Normalized decay rate of $Z \rightarrow q\bar{q}\mathcal{U}$ for the spin-1 unparticle versus $x_3 = 2 - x_1 - x_2$ for different values of $d_{\mathcal{U}} = 1^+, 1.5, 2,$ and 3 , where “ 1^+ ” stands for $1 + \epsilon$ for a small positive ϵ .

$$\frac{d^2 \hat{\sigma}}{d\hat{t} dP_{\mathcal{U}}^2} = \frac{1}{16\pi \hat{s}^2} |\overline{\mathcal{M}}|^2 \frac{1}{2\pi} A_{d_{\mathcal{U}}} \left(\frac{P_{\mathcal{U}}^2}{\Lambda_{\mathcal{U}}^2} \right)^{d_{\mathcal{U}}-2} \frac{1}{\Lambda_{\mathcal{U}}^2} \quad (54)$$

with the following matrix element squared for subprocesses

$$|\overline{\mathcal{M}}(gg \rightarrow g\mathcal{U})|^2 = \frac{1536\pi\alpha_s}{4 \cdot 8 \cdot 8} \lambda_0^2 \frac{(P_{\mathcal{U}}^2)^4 + \hat{s}^4 + \hat{t}^4 + \hat{u}^4}{\hat{s} \hat{t} \hat{u} \Lambda_{\mathcal{U}}^2}, \quad (55)$$

$$|\overline{\mathcal{M}}(q\bar{q} \rightarrow g\mathcal{U})|^2 = \frac{8}{9} g_s^2 \lambda_1^2 \frac{(\hat{t} - P_{\mathcal{U}}^2)^2 + (\hat{u} - P_{\mathcal{U}}^2)^2}{\hat{t} \hat{u}}, \quad (56)$$

$$|\overline{\mathcal{M}}(qg \rightarrow q\mathcal{U})|^2 = -\frac{1}{3} g_s^2 \lambda_1^2 \frac{(\hat{t} - P_{\mathcal{U}}^2)^2 + (\hat{s} - P_{\mathcal{U}}^2)^2}{\hat{s} \hat{t}}, \quad (57)$$

and a formula similar to the last one applies for $\bar{q}g \rightarrow \bar{q}\mathcal{U}$ as well. Note that the gluon fusion process involving λ_0 is further suppressed by dimension counting. Although $P_{\mathcal{U}}^2$ is related to \hat{s} by a kinematic relation similar to Eq. (38), it is not uniquely determined at the hadronic level where $\hat{s} \sim x_1 x_2 s$ with s the center-of-mass energy squared of the colliding hadrons and $x_{1,2}$ are the parton momentum fractions. We found that the peculiar feature of the phase-space factor $A_{d_{\mathcal{U}}}$ as a function of $d_{\mathcal{U}}$ at partonic level is more or less washed out. With only one jet in the final state, not many observables can be constructed. We show in Fig. 8 the energy spectrum of the monojet at the LHC. Since the \hat{s} of each collision is unknown due to parton smearing, the $P_{\mathcal{U}}^2$ of each event cannot be reconstructed. Therefore, it would be difficult to detect the unparticle at the hadronic environment using the monojet signal, in contrast to its original anticipation [2]. One would anticipate that mono-

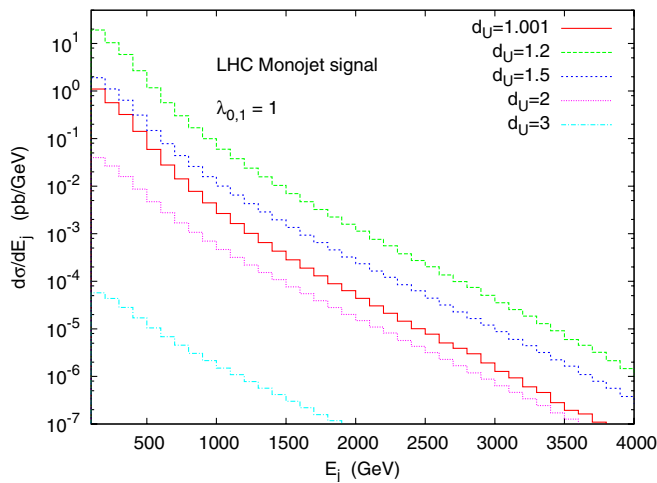


FIG. 8 (color online). Differential cross section $d\sigma/dE_j$ versus E_j for the monojet signal at the LHC, with various $d_{\mathcal{U}}$. We have set $\Lambda_{\mathcal{U}} = 1$ TeV and $\lambda_0 = \lambda_1 = 1$.

photon or mono- Z production plus an unparticle may be more promising at hadronic collisions, because of better experimental resolution for photons and charged leptons. However, one still suffers from the unknown \hat{s} in hadronic collisions. The unparticle information carried by the mono-photon or mono- Z is likely to be washed out by parton smearing as well. Even though we do not consider the case of the spin-2 unparticle here, including them should not alter the conclusion.

D. Present constraints on $\Lambda_{\mathcal{U}}$ from monophoton production at LEP2

LEP collaborations [36] had measured monophoton production in the context of extra dimensions, gauge-mediated SUSY breaking models, and other models that can produce a single photon plus missing energy in the final state. Their limits on monophoton production are similar. We simply take the strongest bound among these LEP results: L3 obtained an 95% C.L. upper limit on $\sigma(e^-e^+ \rightarrow \gamma + X) \simeq 0.2$ pb under the cuts: $E_\gamma > 5$ GeV and $|\cos\theta_\gamma| < 0.97$ at $\sqrt{s} = 207$ GeV. We calculate monophoton plus unparticle production with the same cuts in e^-e^+ collisions with $\sqrt{s} = 207$ GeV versus the unparticle scale $\Lambda_{\mathcal{U}}$ (with a fixed $\lambda_1 = 1$) for $d_{\mathcal{U}} = 1.4, 1.6, 1.8,$ and 2 in Fig. 9. We have also drawn the horizontal line showing the 95% C.L. upper limit (0.2 pb). The limits on $\Lambda_{\mathcal{U}}$ can be read off where the horizontal line intercepts the curves. We tabulate the limits in Table I. Since the production cross section scales as $\lambda_1^2/\Lambda_{\mathcal{U}}^{2d_{\mathcal{U}}-2}$, the limit increases very rapidly when $d_{\mathcal{U}}$ decreases from 2 to 1.4 with λ_1 fixed.

E. Other real emission processes

The first operator in Eq. (30) can involve the left-handed lepton or quark doublet. Therefore, it can give rise to $Z \rightarrow$

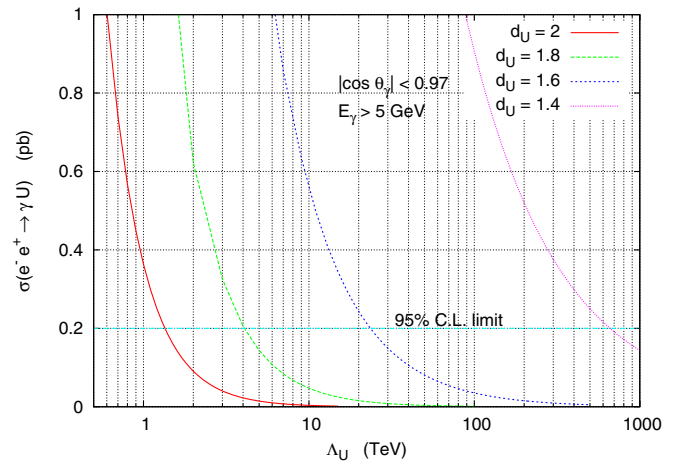


FIG. 9 (color online). Cross sections for monophoton plus unparticle production at the e^-e^+ collider with $\sqrt{s} = 207$ GeV for $d_{\mathcal{U}} = 1.4, 1.6, 1.8,$ and 2 . The horizontal line of 0.2 pb is the 95% C.L. upper limit.

TABLE I. Limits on Λ_U from monophoton production data of $\sigma(e^-e^+ \rightarrow \gamma + X) \approx 0.2$ pb at LEP2 (95% C.L.).

d_U	Λ_U (TeV)
2.0	1.35
1.8	4
1.6	23
1.4	660

$\nu\bar{\nu}U$ and the charged-current process such as $W^- \rightarrow \ell^- \bar{\nu}U$, etc. These decays will affect the invisible width of the Z boson and the missing energy spectrum of the charged W boson decay. An analysis of LEP data for these decays could provide useful constraints on the scale of unparticle physics.

IV. PHENOMENOLOGY: VIRTUAL EXCHANGES AT TREE LEVEL

A. Drell-Yan process

Since the spin-0 operators often bring in a factor proportional to the external light fermion mass in the amplitude, their contributions are in general very small. Here we only consider the contributions from the spin-1 and spin-2 unparticle exchange to the Drell-Yan process.

1. Spin-1 unparticle

The effect of including the spin-1 unparticle virtual exchange in the Drell-Yan process has been studied in Ref. [5]. We include here for completeness. The differential cross section for the Drell-Yan process can be written as

$$\frac{d^2\sigma}{dM_{\ell\ell}dy} = K \frac{M_{\ell\ell}^3}{72\pi s} \sum_q f_q(x_1) f_{\bar{q}}(x_2) \times (|M_{LL}|^2 + |M_{LR}|^2 + |M_{RL}|^2 + |M_{RR}|^2), \quad (58)$$

where $\hat{s} = M_{\ell\ell}^2$ and \sqrt{s} is the center-of-mass energy of the colliding hadrons. $M_{\ell\ell}$ and y are the invariant mass and the rapidity of the lepton pair, respectively, and $x_{1,2} = M_{\ell\ell} e^{\pm y} / \sqrt{s}$. The K factor equals $1 + \frac{\alpha_s}{2\pi} \frac{4}{3} (1 + \frac{4\pi^2}{3})$. The reduced amplitude $M_{\alpha\beta}(\alpha, \beta = L, R)$ is given by

$$M_{\alpha\beta} = \lambda_1^2 Z_{d_U} \frac{1}{\Lambda_U^2} \left(-\frac{\hat{s}}{\Lambda_U^2} \right)^{d_U-2} + \frac{e^2 Q_l Q_q}{\hat{s}} + \frac{e^2 g_\alpha^l g_\beta^q}{\sin^2\theta_w \cos^2\theta_w} \frac{1}{\hat{s} - M_Z^2 + iM_Z\Gamma_Z}. \quad (59)$$

Since $\hat{s} > 0$, the phase factor $\exp(-i\pi d_U)$ in the unparticle 4-fermion contact term will interfere with the photon and Z boson propagator in a rather nontrivial way. This unparticle propagator phase can interfere with both the real photon propagator as well as the real and imaginary parts of the

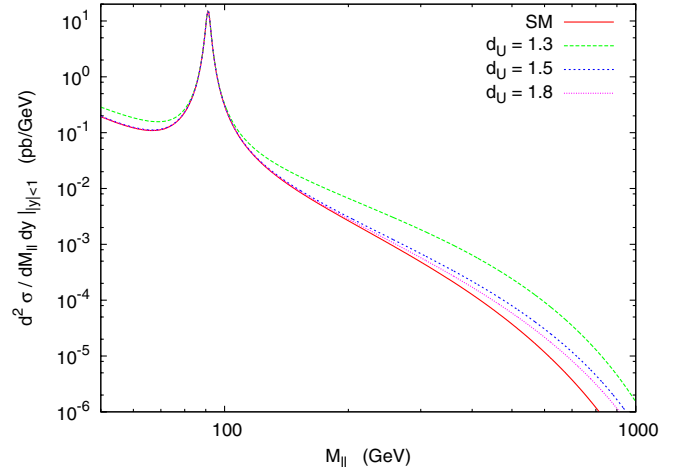


FIG. 10 (color online). Drell-Yan invariant mass distribution for $d_U = 1.3, 1.5,$ and 1.8 at the Tevatron with $\sqrt{s} = 1.96$ TeV. We have chosen $\Lambda_U = 1$ TeV and $\lambda_1 = 1$ for illustration.

unstable Z boson propagator. This gives rise to interesting interference patterns [4]. Despite having a complex phase in the unparticle propagator, it has been demonstrated in [33] using deconstruction that this does not lead to an unstable unparticle. As mentioned earlier, we can allow different couplings in different chirality combinations in the 4-fermion contact interactions. In fact, we are able to reproduce the effects in Ref. [4] using our 4-fermion amplitudes with different chirality couplings. However, it may be difficult to disentangle the fractional differences from the SM prediction in Drell-Yan production due to experimental uncertainties. It may be easier to test the angular distributions and interference patterns in e^-e^+ collisions. We will show the results in the next subsection. For the moment we assume the same coupling in different chirality combinations so that the 4-fermion interactions are vectorlike. In Fig. 10, we depict the Drell-Yan distribution as a function of the invariant mass of the lepton pair for various d_U at the Tevatron. The peculiar effects from the phase-space factor of A_{d_U} for nonintegral values of d_U are evident.

2. Spin-2 unparticle

We also study the effect of exchanging a spin-2 unparticle in Drell-Yan process with the first operator in Eq. (30). A similar pursuit has been performed in [18]. The amplitude for $q(p_1)\bar{q}(p_2) \rightarrow e^-(p_3)e^+(p_4)$ due to unparticle exchange can be adapted from Eq. (32) with the substitutions $p_2 \rightarrow -p_2$ and $p_4 \rightarrow -p_4$:

$$i\mathcal{M}_U = -\frac{i}{8} \lambda_2^2 Z_{d_U} \frac{1}{\Lambda_U^4} \left(-\frac{\hat{s}}{\Lambda_U^2} \right)^{d_U-2} \times [(p_1 - p_2) \cdot (p_3 - p_4) \bar{v}(p_2) \gamma^\mu u(p_1) \bar{u}(p_3) \times \gamma_\mu v(p_4) + \bar{v}(p_2) (\not{p}_3 - \not{p}_4) u(p_1) \bar{u}(p_3) \times (\not{p}_1 - \not{p}_2) v(p_4)]. \quad (60)$$

Let us write the constant prefactor in $i\mathcal{M}_u$ as

$$A = -\frac{1}{8}\lambda_2^2 Z_{d_u} \frac{1}{\Lambda_u^4} \left(-\frac{\hat{s}}{\Lambda_u^2}\right)^{d_u-2}$$

which includes the unparticle phase $\exp(-i\pi d_u)$ for $\hat{s} > 0$. The complete amplitude squared without color or spin average is given by

$$\begin{aligned} \sum |\mathcal{M}|^2 = & \left\{ 4\hat{u}^2(|M_{LL}^{\text{sm}}|^2 + |M_{RR}^{\text{sm}}|^2) + 4\hat{t}^2(|M_{LR}^{\text{sm}}|^2 + |M_{RL}^{\text{sm}}|^2) + 8|A|^2(\hat{t}^4 + \hat{u}^4 - 6\hat{t}^3\hat{u} - 6\hat{t}\hat{u}^3 + 18\hat{t}^2\hat{u}^2) \right. \\ & + 16\frac{e^2 Q_e Q_q}{\hat{s}} \Re(A)(\hat{u} - \hat{t})^3 + 16\frac{e^2}{\sin^2\theta_w \cos^2\theta_w} \Re\left(\frac{A^*}{\hat{s} - M_Z^2 + iM_Z\Gamma_Z}\right) \\ & \left. \times [g_u^e g_u^q (\hat{t}^3 - 3\hat{t}^2\hat{u} - 3\hat{t}\hat{u}^2 + \hat{u}^3) + g_v^e g_v^q (\hat{u} - \hat{t})^3] \right\}, \end{aligned} \quad (61)$$

where

$$M_{\alpha\beta}^{\text{sm}} = \frac{e^2 Q_l Q_q}{\hat{s}} + \frac{e^2 g_\alpha^l g_\beta^q}{\sin^2\theta_w \cos^2\theta_w} \frac{1}{\hat{s} - M_Z^2 + iM_Z\Gamma_Z}, \quad \alpha, \beta = L, R; \quad g_v^f = \frac{g_L^f + g_R^f}{2}, \quad g_a^f = \frac{g_L^f - g_R^f}{2}.$$

The differential cross section for the subprocess is

$$\frac{d\hat{\sigma}}{d\cos\theta^*}(q\bar{q} \rightarrow e^- e^+) = \frac{1}{32\pi\hat{s}} \left(\frac{1}{3} \frac{1}{4} \sum |\mathcal{M}|^2\right), \quad (62)$$

where θ^* is the scattering angle in the parton rest frame, and $\hat{t} = -\frac{\hat{s}}{2}(1 - \cos\theta^*)$, $\hat{u} = -\frac{\hat{s}}{2}(1 + \cos\theta^*)$, and the factor $\frac{1}{3} \frac{1}{4}$ is for the color and spin average of the initial partons. Integrating over $\cos\theta^*$ from -1 to 1 , the subprocess cross section is

$$\begin{aligned} \hat{\sigma}(q\bar{q} \rightarrow e^- e^+) = & \frac{1}{144\pi\hat{s}} \left[\hat{s}^2(|M_{LL}^{\text{sm}}|^2 + |M_{RR}^{\text{sm}}|^2 + |M_{LR}^{\text{sm}}|^2 \right. \\ & \left. + |M_{RL}^{\text{sm}}|^2) + \frac{12}{5}|A|^2\hat{s}^4 \right]. \end{aligned} \quad (63)$$

It is noted that once when $\cos\theta^*$ is integrated, the interference term goes to zero accidentally. Therefore, it is hard to discriminate the effect of the spin-2 unparticle by the invariant mass spectrum because of high suppression of powers of Λ_u in the quantity A . Only the angular distribution can show a discernible effect, but the angular distribution is somewhat smeared out in Drell-Yan production because the central scattering angle is boosted by the partons.

There is another contribution from the subprocess $gg \rightarrow \mathcal{U}^* \rightarrow e^- e^+$ via a tree-level exchange of a spin-2 unparticle. Such a possibility arises from both operators in Eq. (30) in which we assume they have the same couplings. The spin- and color-averaged amplitude squared for this process is given by

$$|\overline{\mathcal{M}}|^2(gg \rightarrow e^- e^+) = 4|A|^2\hat{u}(\hat{u}^2 + \hat{t}^2). \quad (64)$$

The integrated subprocess cross section is

$$\hat{\sigma}(gg \rightarrow e^- e^+) = \frac{1}{40\pi} |A|^2 \hat{s}^3. \quad (65)$$

Folded with parton distribution functions we obtain

$$\begin{aligned} \frac{d^2\sigma}{dM_{\ell\ell} dy} = & K \frac{1}{72\pi s} \left\{ \sum_q f_q(x_1) f_{\bar{q}}(x_2) \right. \\ & \times \left[M_{\ell\ell}^3 (|M_{LL}^{\text{sm}}|^2 + |M_{LR}^{\text{sm}}|^2 + |M_{RL}^{\text{sm}}|^2 + |M_{RR}^{\text{sm}}|^2) \right. \\ & \left. \left. + \frac{12}{5} M_{\ell\ell}^7 |A|^2 \right] + f_g(x_1) f_g(x_2) \frac{18}{5} M_{\ell\ell}^7 |A|^2 \right\}. \end{aligned} \quad (66)$$

It is clear that the invariant mass distribution depends on $|A|^2$ rather than linear in A . Therefore, it needs a rather large coupling for the unparticle operator in order to see the effect, given a large Λ_u . We do not intend to show the invariant mass distribution here because it does not have any special feature. One would rather attempt to look at the angular distribution, which has a linear dependence on A . However, at hadronic machines one has to boost back to the rest frame of the lepton pair in order to obtain the scattering angle. Thus, experimental uncertainties are involved. We would turn to the study of the angular distributions in fermion-pair production at $e^- e^+$ colliders, which is more direct and the center-of-mass energy of the collision is uniquely specified.

B. Fermion-pair production at $e^- e^+$ colliders

The fermion-pair production at $e^- e^+$ colliders can be studied using the amplitude in Eq. (59) and the amplitude squared in Eq. (61) with appropriate color-factor modifications for spin-1 and spin-2 unparticle exchange, respectively.

1. Spin-1 unparticle

The differential cross section including the spin-1 unparticle exchange is given by

$$\frac{d\sigma(e^-e^+ \rightarrow f\bar{f})}{d\cos\theta} = \frac{N_c s}{128\pi} [(1 + \cos\theta)^2 (|M_{LL}|^2 + |M_{RR}|^2) + (1 - \cos\theta)^2 (|M_{LR}|^2 + |M_{RL}|^2)], \quad (67)$$

where $M_{\alpha\beta}$'s are given by Eq. (59).

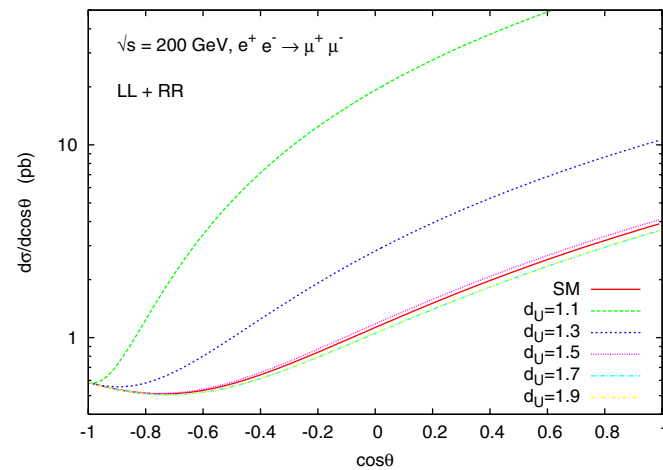
To reiterate, the unparticle 4-fermion contact interactions in Eq. (31) can be different for different chiralities of the fermions. Let us write the contact term between an electron and a fermion f as

$$\mathcal{M}_1^{ef} = \lambda_1^2 Z_{d_U} \frac{1}{\Lambda_U^2} \left(-\frac{P_{d_U}^2}{\Lambda_U^2} \right)^{d_U-2} \sum_{\alpha,\beta=L,R} \eta_{\alpha\beta} (\bar{e}\gamma_\mu P_\alpha e) \times (\bar{f}\gamma^\mu P_\beta f), \quad (68)$$

where $P_{L,R} = (1 \mp \gamma_5)/2$ are the chirality projection operators, and $\eta_{\alpha\beta} = \pm 1, 0$. It is clear from Eq. (67) that different modifications to $M_{\alpha\beta}$ can significantly change the angular distribution, because M_{LL} and M_{RR} are multiplied by $(1 + \cos\theta)^2$ while M_{LR} and M_{RL} are multiplied by $(1 - \cos\theta)^2$. We show in Fig. 11 the angular distribution for $e^-e^+ \rightarrow \mu^-\mu^+$ at $\sqrt{s} = 200$ GeV, with (a) only $LL + RR$ and (b) only $LR + RL$ contact interactions. It is easy to understand why $LL + RR$ is increased in the positive region of $\cos\theta$ while $LR + RL$ is enhanced in the negative $\cos\theta$ region. The forward-backward asymmetry can therefore discriminate various chirality couplings.

The integrated cross section for $e^-e^+ \rightarrow f\bar{f}$ can be obtained as

$$\sigma(e^-e^+ \rightarrow f\bar{f}) = \frac{N_c s}{48\pi} (|M_{LL}|^2 + |M_{RR}|^2 + |M_{LR}|^2 + |M_{RL}|^2). \quad (69)$$



As mentioned before when we calculated the 4-fermion contact interactions, the unparticle propagator has a phase $\exp(-i\pi d_U)$, which can interfere with the real and imaginary parts of the Z boson propagator. We show in Fig. 12 the total cross sections for $e^-e^+ \rightarrow \mu^-\mu^+$ versus \sqrt{s} in the vicinity of the Z pole, with (a) $LL + RR$ contact terms and (b) $LR + RL$ contact terms. Interesting interference patterns can be seen around the Z pole.

2. Spin-2 unparticle

The differential cross section including the spin-2 unparticle exchange can be obtained as

$$\frac{d\sigma(e^-e^+ \rightarrow f\bar{f})}{d\cos\theta} = \frac{1}{32\pi s} \left(N_c \frac{1}{4} \sum |\mathcal{M}|^2 \right), \quad (70)$$

where $\sum |\mathcal{M}|^2$ is given in Eq. (61). We show in Fig. 13 the angular distribution for $e^-e^+ \rightarrow \mu^-\mu^+$ at $\sqrt{s} = 0.5$ TeV with various d_U . For $d_U < 1.3$, features of the spin-2 unparticle exchange can be easily seen.

Integrating over $\cos\theta$ from -1 to 1 , we obtain the total cross section:

$$\sigma(e^-e^+ \rightarrow f\bar{f}) = \frac{N_c}{48\pi s} \left[s^2 (|M_{LL}^{\text{sm}}|^2 + |M_{RR}^{\text{sm}}|^2 + |M_{RL}^{\text{sm}}|^2 + |M_{LR}^{\text{sm}}|^2) + \frac{12}{5} s^4 |A|^2 \right]. \quad (71)$$

Similar to Drell-Yan production the interference term linearly proportional to A goes to zero accidentally. Therefore, the total cross section is not a sensitive probe for the spin-2 unparticle exchange.

C. Diphoton production

Diphoton production at e^-e^+ and hadronic colliders have been proved very useful to detect unknown resonances that can decay into a pair of photons and to search for anomalous diphoton couplings. The spin-2 unparticle

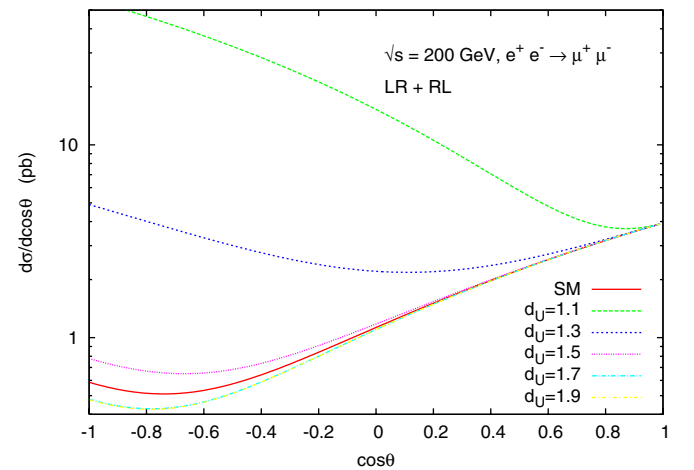


FIG. 11 (color online). Angular distributions for $e^-e^+ \rightarrow \mu^-\mu^+$ with various d_U at $\sqrt{s} = 200$ GeV. The left (right) panel is with $LL + RR$ ($LR + RL$) contact terms plus the SM contributions. We have set $\Lambda_U = 1$ TeV and $\lambda_1 = 1$.

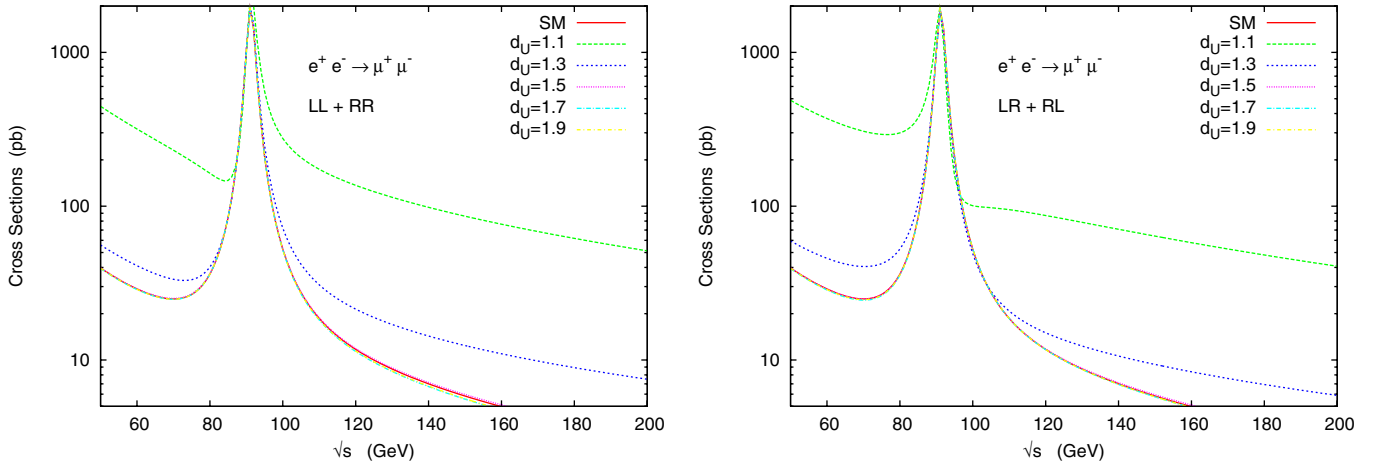


FIG. 12 (color online). Total cross sections for $e^-e^+ \rightarrow \mu^-\mu^+$ versus \sqrt{s} with various d_U . The left (right) panel is with $LL + RR$ ($LR + RL$) contact terms plus the SM contributions. We have set $\Lambda_U = 1$ TeV and $\lambda_1 = 1$.

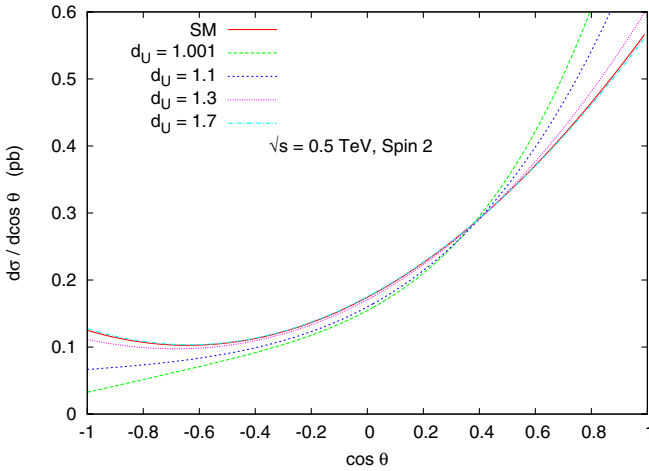


FIG. 13 (color online). Angle distribution for $e^-e^+ \rightarrow \mu^-\mu^+$ with spin-2 unparticle exchange plus SM contributions at $\sqrt{s} = 0.5$ TeV. We have set $\Lambda_U = 1$ TeV and $\lambda_2 = 1$.

can couple to a pair of fermions via the first operator in Eq. (30) and to a pair of photons via the second operator in Eq. (30). There are three contributing Feynman diagrams: the t - and u -channel standard model diagrams and the unparticle s -channel diagram. The amplitude for $f(p_1)\bar{f}(p_2) \rightarrow \gamma(k_1)\gamma(k_2)$ due to the s -channel unparticle exchange is given by

$$\begin{aligned}
 i\mathcal{M}_U = & -\frac{i}{4}\lambda_2^2 Z_{d_U} \left(\frac{-s}{\Lambda_U^2}\right)^{d_U-2} \frac{1}{\Lambda_U^4} \bar{v}(p_2) [\gamma_\rho (p_1 - p_2)_\sigma \\
 & + \gamma_\sigma (p_1 - p_2)_\rho] u(p_1) \epsilon_\mu(k_1) \epsilon_\nu(k_2) \\
 & \times [g^{\mu\nu} (k_1^\rho k_2^\sigma + k_2^\rho k_1^\sigma) \\
 & + k_1 \cdot k_2 (g^{\rho\mu} g^{\sigma\nu} + g^{\sigma\mu} g^{\rho\nu}) \\
 & - k_1^\nu (k_2^\rho g^{\sigma\mu} + k_2^\sigma g^{\rho\mu}) - k_2^\mu (k_1^\rho g^{\sigma\nu} + k_1^\sigma g^{\rho\nu})].
 \end{aligned} \tag{72}$$

Again, let us denote the constant prefactor in $i\mathcal{M}_U$ as

$$A' = -\frac{1}{4}\lambda_2^2 Z_{d_U} \left(\frac{-s}{\Lambda_U^2}\right)^{d_U-2} \frac{1}{\Lambda_U^4}. \tag{73}$$

The spin- and color-averaged amplitude squared is given by

$$\begin{aligned}
 |\overline{\mathcal{M}}|^2 = & \frac{1}{4} \frac{1}{N_c} \left\{ 8e^4 Q_f^4 \left(\frac{u}{t} + \frac{t}{u}\right) + 32ut(u^2 + t^2) |A'|^2 \right. \\
 & \left. + 32e^2 Q_f^2 (u^2 + t^2) \Re(A') \right\}.
 \end{aligned} \tag{74}$$

The differential cross section is given by

$$\frac{d\sigma}{d|\cos\theta_\gamma|} (f\bar{f} \rightarrow \gamma\gamma) = \frac{1}{32\pi s} |\overline{\mathcal{M}}|^2, \tag{75}$$

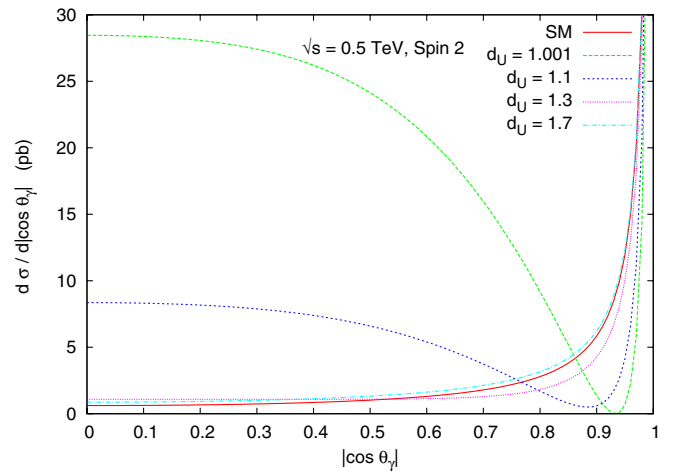


FIG. 14 (color online). The differential cross section $\frac{d\sigma}{d|\cos\theta_\gamma|} \times (e^-e^+ \rightarrow \gamma\gamma)$ versus $|\cos\theta_\gamma|$ at $\sqrt{s} = 0.5$ TeV with a spin-2 unparticle virtual exchange plus standard model contributions. λ_2 is set at 5 for visibility and $\Lambda_U = 1$ TeV.

where $0 \leq |\cos\theta_\gamma| \leq 1$ because of identical photons in the final state. We show the angular distribution in Fig. 14. In the SM, the angular distribution is very forward with the majority of the cross section at $|\cos\theta_\gamma|$ close to 1. When d_U is less than 1.2 the majority comes from the central

region and a dip is formed around $|\cos\theta_\gamma| \approx 0.9$. It is because of the spin-2 structure of the operator. The angular variable $|\cos\theta_\gamma|$ can be integrated from 0 to a cutoff z because of the collinear divergence of the SM cross section at $|\cos\theta_\gamma| = 1$. We obtain the integrated cross section as

$$\sigma(f\bar{f} \rightarrow \gamma\gamma)|_{0 \leq |\cos\theta_\gamma| < z} = \frac{1}{32\pi s} \frac{1}{4N_c} \left\{ 8e^4 Q_f^4 \left[-2z - 2 \log \left| \frac{1-z}{1+z} \right| \right] + 32s^4 \left(\frac{z}{8} - \frac{z^5}{40} \right) |A'|^2 + 32e^2 Q_f^2 s^2 \left(\frac{z}{2} + \frac{z^3}{6} \right) \Re(A') \right\}. \quad (76)$$

We show the total cross section of $e^-e^+ \rightarrow \gamma\gamma$ with a spin-2 unparticle exchange versus the center-of-mass energy in Fig. 15 with an angular cut of $|\cos\theta_\gamma| < 0.95$. We have set $\Lambda_U = 1$ TeV and $\lambda_2 = 1$. The cross section starts to show visible deviations when \sqrt{s} is around 0.5 TeV.

D. Experimental constraints on unparticle scale Λ_U

Since the spin-1 unparticle exchanges will lead to 4-fermion contact interactions, we can use the existing limits on 4-fermion contact interactions [37,38] to constrain the unparticle scale Λ_U . We can compare Eq. (68) with the conventional 4-fermion contact interactions

$$\mathcal{L}_{4f} = \frac{4\pi}{\Lambda^2} \sum_{\alpha, \beta=L,R} \eta_{\alpha\beta} (\bar{e}\gamma_\mu P_\alpha e)(\bar{f}\gamma^\mu P_\beta f), \quad (77)$$

which results in the following equality:

$$\lambda_1^2 Z_{d_U} \frac{1}{\Lambda_U^2} \left(-\frac{P_U^2}{\Lambda_U^2} \right)^{d_U-2} = \frac{4\pi}{(\Lambda^{95})^2}, \quad (78)$$

where Λ^{95} s are the 95% C.L. limits on the $eeqq$ contact interaction scales obtained by combining global data on fermion-pair production at LEP, Drell-Yan production at

the Tevatron, deep-inelastic scattering at HERA, and a number of low-energy parity-violating experiments [37].

Instead of performing a full analysis, we do a simple estimate here by putting a fixed value for P_U^2 into Eq. (78). Since the limits are dominated by the LEP2 data [37] when parity-conserving operators are considered, a fixed value of $P_U^2 \approx (0.2 \text{ TeV})^2$ is chosen. Other choices are possible but will not affect our results significantly. The best limit is on the LL chirality because the parity-violating experiments, especially the atomic-parity violation, are very stringent: $\Lambda_{LL}^{95}(eeuu) \approx 23 \text{ TeV}$ while $\Lambda_{LL}^{95}(eedd) \approx 26 \text{ TeV}$. When parity-conserving combinations are considered, the limits are lowered: $\Lambda_{VV}^{95}(eeuu) \approx 20 \text{ TeV}$, $\Lambda_{VV}^{95}(eedd) \approx 12 \text{ TeV}$, and $\Lambda_{AA}^{95}(eedd) \approx \Lambda_{VV}^{95}(eeuu) = 15 \text{ TeV}$. We rescale these 4-fermion contact interaction limits to the limits on the unparticle scale Λ_U using Eq. (78), with $\lambda_1 = 1$ and $P_U^2 = (0.2 \text{ TeV})^2$. The results are shown in Fig. 16. Note that we have ignored the phase in the unparticle propagator in the analysis. The limits obtained are similar to those obtained from the single-photon production at LEP2.

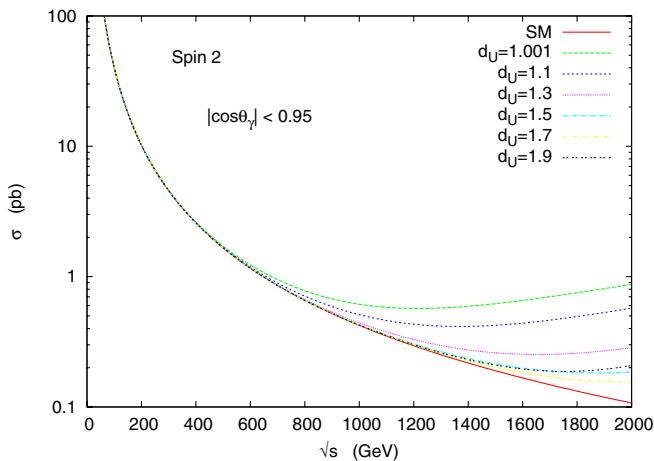


FIG. 15 (color online). Total cross section for $e^-e^+ \rightarrow \gamma\gamma$ with spin-2 unparticle exchange plus standard model contributions versus center-of-mass energy for different values of d_U . We have set $\Lambda_U = 1$ TeV and $\lambda_2 = 1$.

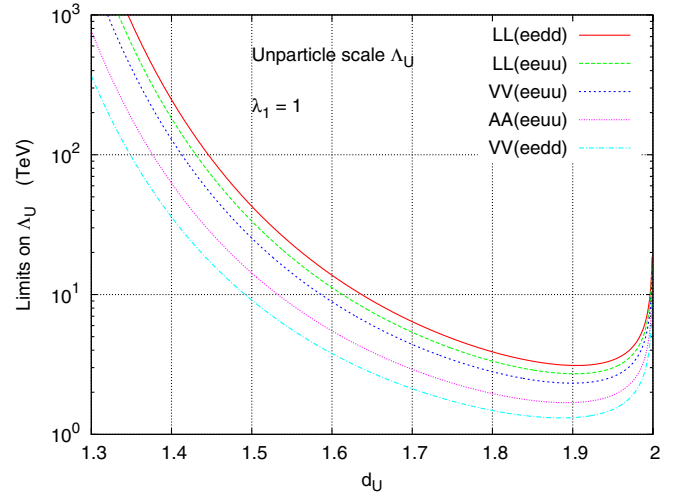


FIG. 16 (color online). Rescaled limits from existing 4-fermion contact interactions. LL means only left-left chirality is considered while VV means $LL + RR + LR + RL$ and AA means $LL + RR - LR - RL$. We have chosen $P_U^2 \approx (0.2 \text{ TeV})^2$.

The estimates here are rather crude, because we have substituted the factor $P_{\mathcal{U}}^2$ by a constant $(0.2 \text{ TeV})^2$, which should be good for a crude estimate. In principle, a different $P_{\mathcal{U}}^2$ is needed for analysis of each high-energy process. An updated global analysis using $P_{\mathcal{U}}^2$ dependent amplitudes is necessary for more accurate limits. Similarly, another global analysis is needed for constraining the spin-2 unparticle exchange. We note that a recent paper [22] has also derived some limits of the unparticle scale.

V. CONCLUSIONS

Scale invariance or the enlarged conformal invariance is an attractive symmetry, but is not realized in the low-energy visible world. Perhaps, below a sufficient high-energy scale an exact scale invariant hidden sector may exist. Such a strictly scale invariant sector may couple weakly to the SM particles such that we may be able to probe it via high-energy processes at the LHC and ILC. Operators $\mathcal{O}_{\mathcal{U}}$ of a scale invariant sector with a general nonintegral scaling dimension $d_{\mathcal{U}}$ has a phase space that looked like a $d_{\mathcal{U}}$ number of invisible massless particles. Therefore, a typical reaction that involves emission of the unparticle in the final state gives rise to missing energy signals in the detectors. We have studied a number of processes that involve emission of the unparticle in the final state, including $e^-e^+ \rightarrow \gamma\mathcal{U}$, $Z\mathcal{U}$ at the ILC and $Z \rightarrow f\bar{f}\mathcal{U}$ at the Z -pole, as well as the monojet production at the LHC. We found that the energy distribution of the single photon or the single Z at ILC and the missing energy distribution in $Z \rightarrow f\bar{f}\mathcal{U}$ can discriminate the scaling dimension $d_{\mathcal{U}}$. However, the monojet energy spectrum is not so sensitive to $d_{\mathcal{U}}$ because of the washout by parton smearing.

We also formulate the virtual exchange of unparticles between SM particles. We have shown that spin-1 unparticle exchange between two fermions gives rise to contact 4-fermion interactions, which scale as $(\hat{s}/\Lambda_{\mathcal{U}}^2)^{d_{\mathcal{U}}-1}$ and thus differ from the conventional one because of the peculiar scaling dimension $d_{\mathcal{U}}$. Spin-2 unparticle exchange gives rise to another form of 4-fermion interactions. We have used Drell-Yan production at hadronic colliders and fermion-pair production at e^-e^+ colliders to study the interference of the unparticle-exchange amplitudes with the SM amplitudes. One peculiar feature of the unparticle propagator is the phase factor $\exp(-i\pi d_{\mathcal{U}})$ which may interfere nontrivially with the Z boson propagator. We have demonstrated the intriguing interference effects in great detail in fermion-pair production in e^-e^+ collisions. Finally, we have also studied diphoton production, which also shows the peculiar feature of the phase of unparticle propagator.

Unparticles can be conjectured as a generalization of extra dimensions. The number of extra dimensions only take on integral values while the scaling dimension of the unparticle can take on any, even nonintegral values. We

speculate on a relation $d_{\mathcal{U}} = n/2 + 1$ that relates the scaling dimension to the number of large extra dimensions. Therefore, unparticle physics is another program just as important as extra dimensions in the goals of the LHC.

Before we end, we offer a number of comments as follows.

- (1) The calculation of diphoton production can be easily extended to other diboson production, such as ZZ and W^+W^- , at e^-e^+ and hadronic machines. Likewise, one can study the unparticle effect in the gauge boson scattering [14].
- (2) The peculiar phase factor in the unparticle propagator can be used as a strong phase that is required in the CP violation studies [7] of the B -meson system.
- (3) It is more natural to assume that the unparticle sector is flavor blind. Flavor changing coupling of the SM particles with the unparticle can then be induced at 1-loop via W -boson exchange as was done in the second paper in [7]. Direct flavor changing couplings of the SM fermions with an unparticle will suffer strong constraints from low-energy flavor changing processes [6,7,10–12,16]. These constraints would push unparticle physics out of reach at the LHC.
- (4) Dijet production at hadronic colliders is also sensitive to unparticle exchange. It would be similar to diphoton production. One would expect enhancement of cross section at high invariant mass of the dijet.
- (5) Our formulas for 4-fermion contact interactions can be applied to other areas, e.g., the ep deep-inelastic scattering [8], low-energy parity-violating experiments, $D - \bar{D}$ or $B - \bar{B}$ mixings [6,7,11], and atomic-parity violation experiments [27].
- (6) Quarkonium decays can also constrain the unparticle by their invisible widths and by the decay mode of $\gamma + \text{nothing}$.
- (7) Astrophysics places constraints on real emission of unparticles. In principle, emission of unparticles in supernova, neutron stars, or some other astrophysical systems can lead to substantial cooling other than that by neutrinos. Therefore, using the experimentally measured cooling rates one can constrain the unparticle scale. Various limits of the unparticle scale have been estimated in [15] from the supernova SN 1987A data as well as from other cosmological considerations.
- (8) The spin-1 unparticle contribution to the lepton anomalous magnetic moment at 1 loop has been calculated [5]. It should be possible to extend the calculation to the spin-2 case as well. The effect is expected to be minuscule, however.
- (9) Besides the 2-point function, the momentum part of a 3-point or in general n -point function is known for a conformal field theory in 4 dimensions up to an

overall constant. Can one determine the overall constant for the 3-point or in general n -point function for the unparticle operators? We will leave this to those with more ambitious minds.

Phenomenology of unparticle physics is quite rich. While the underlying theory of the unparticle is still needed to be unraveled by theorists, experimentalists could detect such a hidden scale invariant sector when the behemoth LHC machine becomes online in the year 2008.

ACKNOWLEDGMENTS

This research was supported in part by the NSC under Grant No. NSC 95-2112-M-007-001, NCTS, and U.S. DOE under Grant No. DE-FG02-84ER40173.

APPENDIX: FUNCTIONS F , G , AND H

These functions appeared in $f\bar{f} \rightarrow Z\mathcal{U}$ for the spin-2 unparticle \mathcal{U} .

$$(F, G, H) = (F_0, G_0, H_0) + \frac{1}{P_{\mathcal{U}}^2}(F_2, G_2, H_2) + \frac{1}{P_{\mathcal{U}}^4}(F_4, G_4, H_4)$$

with

$$\begin{aligned} F_0(t, u) &= 2t^2u^2[16M_Z^6 + P_{\mathcal{U}}^2(7t^2 + 12tu + 7u^2) - 3(3t^3 + 11t^2u + 11tu^2 + 3u^3) + 6M_Z^4(7P_{\mathcal{U}}^2 - 2(t + u)) \\ &\quad + M_Z^2(14P_{\mathcal{U}}^4 - 15t^2 - 44tu - 15u^2 + 2P_{\mathcal{U}}^2(t + u))], \\ G_0(t, u) &= 4tu\{6M_Z^6(P_{\mathcal{U}}^2 - t - u)(t + u) + M_Z^4[9t^3 + 7t^2u + 7tu^2 + 9u^3 + 15P_{\mathcal{U}}^4(t + u) - 2P_{\mathcal{U}}^2(12t^2 + 19tu + 12u^2)] \\ &\quad + tu[6P_{\mathcal{U}}^6 - 9P_{\mathcal{U}}^4(t + u) - P_{\mathcal{U}}^2(t^2 + 12tu + u^2) + 6(t^3 + 6t^2u + 6tu^2 + u^3)] \\ &\quad + M_Z^2[-3t^4 + 25t^3u + 58t^2u^2 + 25tu^3 - 3u^4 + 6P_{\mathcal{U}}^6(t + u) - P_{\mathcal{U}}^4(15t^2 + 2tu + 15u^2) \\ &\quad + 2P_{\mathcal{U}}^2(6t^3 - 11t^2u - 11tu^2 + 6u^3)]\}, \\ H_0(t, u) &= 24M_Z^6tu(-P_{\mathcal{U}}^2 + t + u)^2 - 6M_Z^4tu[-9P_{\mathcal{U}}^6 + 24P_{\mathcal{U}}^4(t + u) - P_{\mathcal{U}}^2(21t^2 + 38tu + 21u^2) \\ &\quad + 2(3t^3 + 5t^2u + 5tu^2 + 3u^3)] - M_Z^2[3P_{\mathcal{U}}^8(t^2 - 12tu + u^2) - 2tu(t + u)^2(6t^2 - 29tu + 6u^2) \\ &\quad - 6P_{\mathcal{U}}^6(t^3 - 16t^2u - 16tu^2 + u^3) + 54P_{\mathcal{U}}^2tu(t^3 + t^2u + tu^2 + u^3) \\ &\quad + P_{\mathcal{U}}^4(3t^4 - 102t^3u - 166t^2u^2 - 102tu^3 + 3u^4)] + tu[6P_{\mathcal{U}}^{10} - 18P_{\mathcal{U}}^8(t + u) - 12P_{\mathcal{U}}^4(t + u)^3 \\ &\quad + 3P_{\mathcal{U}}^6(7t^2 + 12tu + 7u^2) - 18tu(t^3 + 5t^2u + 5tu^2 + u^3) + P_{\mathcal{U}}^2(3t^4 + 32t^3u + 78t^2u^2 + 32tu^3 + 3u^4)], \\ F_2(t, u) &= 2t^2u^2(t + u)[-8M_Z^4(t + u) + 4M_Z^2(t^2 + 3tu + u^2) + 3(t^3 + 5t^2u + 5tu^2 + u^3)], \\ G_2(t, u) &= -4t^2u^2(t + u)[-10M_Z^4(t + u) + 2M_Z^2(3t^2 + 7tu + 3u^2) + 3(t^3 + 5t^2u + 5tu^2 + u^3)], \\ H_2(t, u) &= 2t^2u^2(t + u)^2[-12M_Z^4 + 8M_Z^2(t + u) + 3(t^2 + 4tu + u^2)], \\ F_4(t, u) &= H_4(t, u) = -\frac{1}{2}G_4(t, u) = -2t^2u^2(t + u)^3(t^2 + u^2 - M_Z^2(t + u)). \end{aligned}$$

The following relations are found to be satisfied by these functions

$$F_2 + G_2 + H_2 = 0, \quad F_4 + G_4 + H_4 = 0.$$

-
- [1] S. Coleman and E. Weinberg, Phys. Rev. D **7**, 1888 (1973).
 - [2] H. Georgi, Phys. Rev. Lett. **98**, 221601 (2007).
 - [3] T. Banks and A. Zaks, Nucl. Phys. **B196**, 189 (1982).
 - [4] H. Georgi, Phys. Lett. B **650**, 275 (2007).
 - [5] K. Cheung, W. Y. Keung, and T. C. Yuan, Phys. Rev. Lett. **99**, 051803 (2007).
 - [6] M.-x. Luo and G.-h. Zhu, arXiv:0704.3532.
 - [7] C.-H. Chen and C.-Q. Geng, arXiv:0705.0689; arXiv:0706.0850 [Phys. Rev. D (to be published)].
 - [8] G.-J. Ding and M.-L. Yan, arXiv:0705.0794; arXiv:0706.0325.
 - [9] Y. Liao, arXiv:0705.0837.
 - [10] T. M. Aliev, A. S. Cornell, and N. Gaur, J. High Energy Phys. **07** (2007) 072; arXiv:0705.4542.
 - [11] X.-Q. Li and Z.-T. Wei, Phys. Lett. B **651**, 380 (2007).
 - [12] C.-D. Lu, W. Wang, and Y.-M. Wang, arXiv:0705.2909.
 - [13] P. J. Fox, A. Rajaraman, and Y. Shirman, arXiv:0705.3092.
 - [14] N. Greiner, arXiv:0705.3518.

- [15] H. Davoudiasl, arXiv:0705.3636.
- [16] D. Choudhury, D.K. Ghosh, and Mamta, arXiv:0705.3637.
- [17] S.-L. Chen and X.-G. He, arXiv:0705.3946; S.-L. Chen, X.-G. He, and H.C. Tsai, arXiv:0707.0187.
- [18] P. Mathews and V. Ravindran, arXiv:0705.4599.
- [19] S. Zhou, arXiv:0706.0302.
- [20] Y. Liao and J.-Y. Liu, arXiv:0706.1284.
- [21] R. Foadi, M.T. Frandsen, T.A. Rytrov, and F. Sannino, arXiv:0706.1696.
- [22] M. Bander, J.L. Feng, A. Rajaraman, and Y. Shirman, arXiv:0706.2677.
- [23] T.G. Rizzo, arXiv:0706.3025.
- [24] H. Goldberg and P. Nath, arXiv:0706.3898.
- [25] G. Mack, Commun. Math. Phys. **55**, 1 (1977).
- [26] E. Eichten, K.D. Lane, and M.E. Peskin, Phys. Rev. Lett. **50**, 811 (1983).
- [27] V.D. Barger, K.m. Cheung, K. Hagiwara, and D. Zeppenfeld, Phys. Rev. D **57**, 391 (1998).
- [28] K. Cheung, arXiv:hep-ph/0409028.
- [29] K. Cheung, Phys. Lett. B **460**, 383 (1999).
- [30] N. Arkani-Hamed, S. Dimopoulos, and G.R. Dvali, Phys. Lett. B **429**, 263 (1998).
- [31] T. Han, J.D. Lykken, and R.J. Zhang, Phys. Rev. D **59**, 105006 (1999).
- [32] G.F. Giudice, R. Rattazzi, and J.D. Wells, Nucl. Phys. **B544**, 3 (1999).
- [33] M.A. Stephanov, arXiv:0705.3049 [Phys. Rev. D (to be published)].
- [34] K.m. Cheung and W.Y. Keung, Phys. Rev. D **60**, 112003 (1999).
- [35] K.m. Cheung, W.Y. Keung, and T.C. Yuan, Phys. Rev. Lett. **76**, 877 (1996); S. Fleming, Phys. Rev. D **50**, 5808 (1994); K. Hagiwara, A.D. Martin, and W.J. Stirling, Phys. Lett. B **267**, 527 (1991).
- [36] A. Heister *et al.* (ALEPH Collaboration), Eur. Phys. J. C **28**, 1 (2003); J. Abdallah *et al.* (DELPHI Collaboration), Eur. Phys. J. C **38**, 395 (2005); P. Achard *et al.* (L3 Collaboration), Phys. Lett. B **587**, 16 (2004); G. Abbiendi *et al.* (OPAL Collaboration), Eur. Phys. J. C **18**, 253 (2000).
- [37] K.m. Cheung, Phys. Lett. B **517**, 167 (2001).
- [38] Particle Data Group, J. Phys. G **33**, 1 (2006).